TOPICAL REVIEW

A review on intense pulsed light process as post-treatment for metal oxide thin films and nanostructures for device application

To cite this article: Youngwook Noh *et al* 2022 *Nanotechnology* **33** 272001

IOP Publishing Nanotechnology
Nanotechnology 33 (2022) 272001 (23pp) https://doi.org/10.1088/1361-6528/ac6314

Topical Review

A review on intense pulsed light process as post-treatment for metal oxide thin films and nanostructures for device application

Youngwook Noh[1], Gyu Young Kim[1], Horim Lee[1], Jaehak Shin[1], Kunsik An[2], Manoj Kumar[3] and Dongjin Lee[1]

[1] Department of Mechanical Design and Production Engineering, Konkuk University, Seoul, Republic of Korea
[2] Department of Mechatronics Engineering, Konkuk University, Chungju, Republic of Korea
[3] Department of Physics, Starex University, Haryana, India

E-mail: djlee@konkuk.ac.kr

Received 31 October 2021, revised 22 February 2022
Accepted for publication 30 March 2022
Published 20 April 2022

Abstract

The intense pulsed light (IPL) post-treatment process has attracted great attention in the device fabrication due to its versatility and rapidity particularly for solution process functional structures in devices, flexible/printed electronics, and continuous manufacturing process. The metal oxide materials inherently have multi-functionality and have been widely used in form of thin films or nanostructures in device application such as thin film transistors, light emitting diodes, solar cells, supercapacitors, etc. The IPL treatment enhances the physical and/or chemical properties of the functional metal oxide through photothermal effects. However, most metal oxides are transparent to most range of visible light and require more energy for post-treatment. In this review, we have summarized the IPL post-treatment processes for metal oxide thin films and nanostructures in device applications. The sintering and annealing of metal oxides using IPL improved the device performances by employing additional light absorbing layer or back-reflector. The IPL process becomes an innovative versatile post-treatment process in conjunction with multi-functional metal oxides in near-future device applications.

Keywords: intense pulsed light (IPL), metal oxide, post-treatment, thin films, nanostructures, annealing, sintering

(Some figures may appear in colour only in the online journal)

1. Introduction

Intense pulsed light (IPL) is the high-power light emitted from a xenon flash lamp. Its duration is on range of milli-seconds and wavelength is on range of 200–1000 nm including the visible light [1]. For this reason, the IPL process is also called the flash lamp process [2–8]. The IPL system consists of a xenon flash lamp, a reflector, a capacitor, and pulse controller as shown in figure 1(a) [9]. The IPL process is performed with pulse time (t), off time (d), energy intensity, and number of pulses as process variables as shown in figure 1(b) [10]. This makes it possible to manipulate the waveforms so that a variety of process conditions can be applied to different types of functional materials for device application. The temperature change in the functional material according to the waveform in figure 1(b) is shown in figure 1(c) [10]. The temperature increases rapidly during pulse time and decreases rapidly during off time. It can maintain low temperature by repeating increase and decrease according to the repeated pulse. This characteristic of IPL has attracted great attention in device fabrication for a variety of applications.

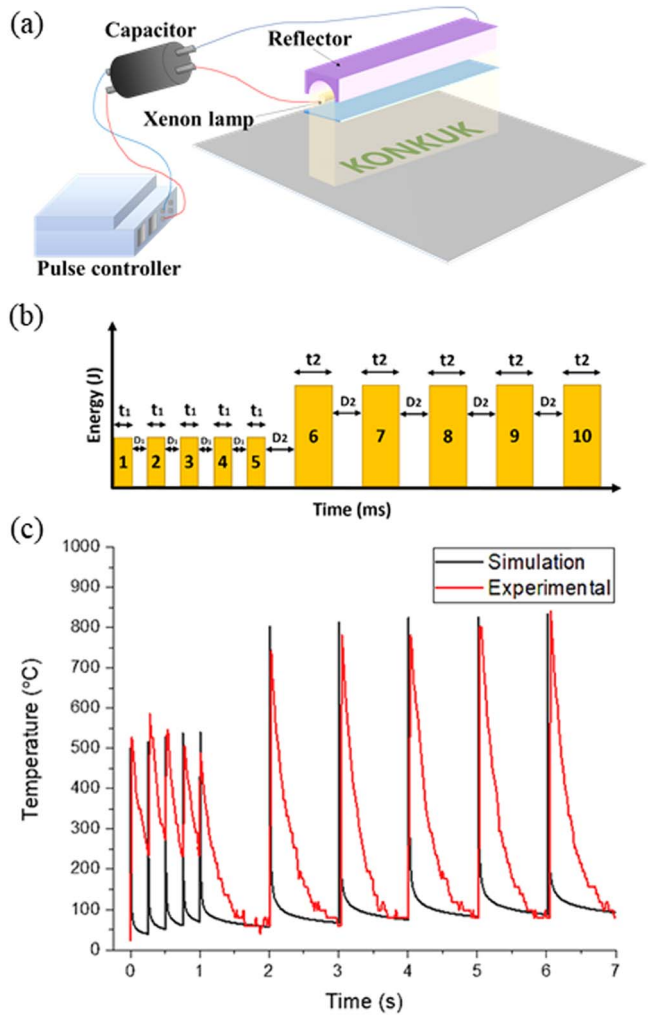

Figure 1. IPL post-treatment system: (a) schematic of IPL sintering system and xenon flash lamp setup. (b) Conditions of IPL, (c) numerical and experimental results demonstrating the maximum temperature rise occurring at the perovskite film. Reprinted with permission from [10]. Copyright (2020) American Chemical Society.

The IPL post-treatment process has a variety of advantages. First, it can be applied to various types of functional materials such as metals [11–18], semiconductors [19–24], and dielectrics [25–28] due to wide wavelength characteristics. Each material has its own light absorption, followed by heat emission, characteristics depending on the wavelength. Contrary to ultraviolet (UV) [29–31] or laser [32–34], which has limited wavelength in its spectrum, IPL irradiates the light with broadband wavelength. Therefore, there is no need to tune the equipment for different types of functional materials to obtain substantial effect. Second, it can be instantaneously processed in an ambient environment. The functional material exposed to IPL absorbs most of the light energy at the top of the absorbable layer. Then, the temperature rises rapidly due to strong pulse energy. Since the other part of the material is maintained almost at room temperature, the heat generated at the top is quickly conducted to the entire device by heat conduction. Even with continuous irradiation of IPL, the device can maintain a temperature close to room temperature. This allows the IPL process to be processed at room temperature without significant restrictions on the ambient environment. Therefore, the IPL process is compatible with flexible/printed electronics and continuous manufacturing processing. The substrates used in flexible/printed electronics are mainly polymeric materials that are vulnerable to heat. Heat generated by the IPL irradiation is rapidly released through the entire substrate by heat conduction, thereby minimizing damage to the substrate. In addition, the functional materials should be post-processed rapidly online while the substrate is transported to enhance the productivity in continuous manufacturing process. IPL not only enables instantaneous post-processing even on the material being transported, but is also more effective in heat dissipation not to damage the continuously moving substrates.

In conjunction with metal nanostructure applied in printed electronics, IPL process has been reviewed in previous publication [35]. The thermal method had been conventionally used to sinter or anneal the metal nanostructures [36–40]. However, it requires high-temperature facility and long process time to obtain desired effects. Infrared [41, 42], laser [43, 44], electrical [45, 46], plasma [47, 48] and microwave [49, 50] post-treatment methods have been studied to address these issues. Among them, the IPL post-treatment method has been proposed as the most suitable mean in device fabrication. The silver and copper nanostructures in the form of nanoparticle [11–18] and nanowire [51–56] were mainly used as conductive materials in IPL post-treatment. The IPL process has been utilized to modify characteristics of the functional materials adequately. First, post-treatment such as sintering and annealing are possible due to the photothermal effect. The photothermal effect is a physical phenomenon in which the light energy is absorbed when light energy is irradiated to a material. The strong energy of IPL induces the release of a lot of thermal energy instantaneously in the material. The released thermal energy can replace the thermal post-treatment process in vicinity of high temperature region. The sintering or annealing of the functional materials is possible depending on the amount of heat energy. The sintering is the process of compacting and forming a solid mass of material by heat or pressure without melting entire material to the point of liquefaction. The sintering was mainly used for nanostructured metal and metal oxide materials in electronics field to improve electrical conductivity by interconnecting them. The annealing is the process of recrystallizing a material to make it softer. The annealing was mainly used for functional thin film and patterned structure to increase the crystallinity of a material in electronics field, resulting in the change of electrical properties.

Despite the desired effects, metal oxide materials have two limitations to apply IPL process. First, contrary to metal composed of metallic bonds, metal oxide are compounds composed of ionic bonds between metal cations and oxygen anions. The strong ionic bonding force requires higher energy in the heat treatment process than metal bond. That is, heat treatment of metal oxides is difficult to attain in thermal processing equipment for metals. Second, metal oxide has

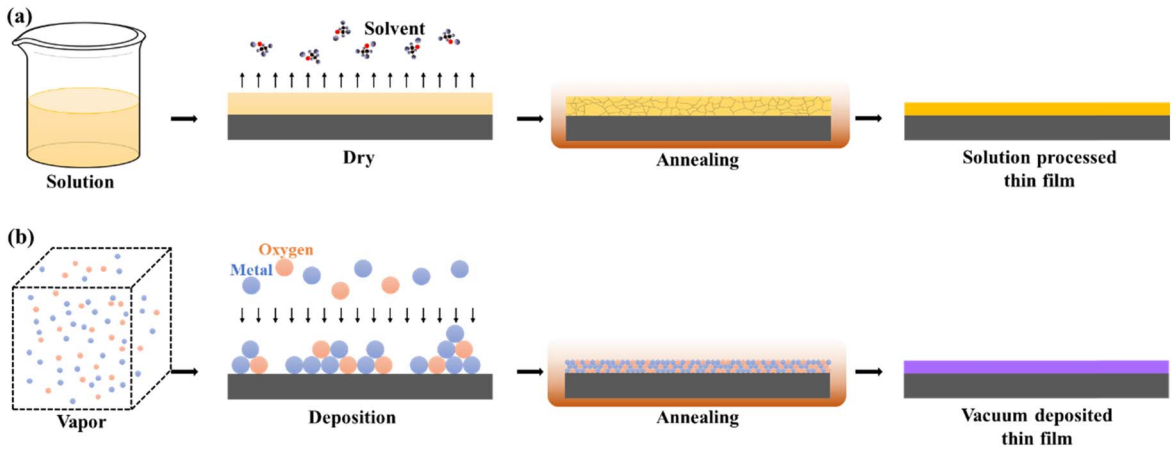

Figure 2. Comparison of solution and vacuum processes for depositing thin film: (a) solution processed thin film, (b) vacuum deposited thin film.

higher band gap than metal (3 eV or greater). Due to the larger band gap than visible light photon energy, visible light cannot be absorbed and passed through, making metal oxide thin films and nanostructures appear transparent. The free electrons in metals have high absorbance for visible light whose energy is 1–3 eV. Metals with high absorbance are effectively heat treated even at low energy of IPL. However, metal oxides are less efficient because they can only absorb part of the UV region of the IPL's spectrum.

In this review, we summarize and review research on the IPL post-treatment process of metal oxide and its device applications in form of thin films and nanostructures. Due to the high heat treatment temperature and low absorbance of metal oxide materials, various methods have been studied to increase the efficiency of the IPL process. In addition, the IPL process could be applied to various processes related to thermal processes as well as heat treatment. IPL process based on metal oxide materials were reviewed for both solution process and vacuum deposition.

2. IPL post-treatment of metal oxide thin films

The metal oxide is a material composed of an ionic marriage between a metal and an oxygen atom. Since indium oxide (In_2O_3) and tin dioxide (SnO_2) were introduced into thin film transistors (TFT), they have attracted much attention as semiconductor materials [57]. Recently, interest in metal oxide thin films has been amplified by realizing high-performance amorphous oxide TFTs based on amorphous indium gallium zinc oxide (a-IGZO). The technology developed rapidly as the research revealed the characteristics of oxide TFTs, including high field-effect mobility in the amorphous phase, high uniformity over a large area, and high optical transparency [58]. With the development of metal oxide thin films, metal oxide TFTs have been commercialized as a basic driving device for liquid crystal displays, contributing greatly to the display industry. The indium tin oxide (ITO) thin film, in which electricity flows through oxygen vacancies by mixing In_2O_3 and SnO_2, enabled the electric products that require transparent electrodes such as touch panel [59], light emitting diodes (LED) [60], and dye-sensitive solar cells (DSSC) [61]. In general, metal oxide thin films are mainly manufactured by a solution process or vacuum deposition process as shown in figure 2. The vacuum deposition process is already commercialized to attain deposition of metal oxide thin films. These days, a solution process is of great interest in the field of flexible/printed electronics, where a precursor is coated on a substrate followed by post-treatment to endow adequate properties. In this section, metal oxide thin films formed by solution process and vacuum deposition followed by IPL post-treatment to improve device performance were reviewed.

2.1. Solution processed thin films

Metal oxide thin films coated by solution process techniques are discussed for IPL annealing. Solution process uses organic or inorganic materials in solution phase. It has the advantage of being able to control the atomic composition of the formed material and not requiring special and complex equipment unlike conventional vacuum deposition techniques. In addition, the solution phase precursor can be applied to various techniques such as ink-jet [62], screen printing [63], gravure printing [38], slot-die coating [64], spray coating [65], and spin coating [66], etc. Although the advantages of solution processing are clear, a low performance of solution-processed devices, processing time, and high-temperature processing are still obstacles for scale-up production. The IPL process can be an alternative to these problems.

The efficient photo-annealing effect of active layers in indium gallium zinc oxide (IGZO) metal oxide TFT on silicon dioxide (SiO_2)/silicon (Si) wafer through IPL irradiation was demonstrated [19]. Although IGZO is transparent to visible light, it can be annealed by heat absorption on SiO_2/Si wafer. Systematic characterization of semiconductor thin films confirmed that IPL irradiation immediately generated sufficient thermal energy to facilitate the complete conversion from sol-gel to solid thin films. The performance of the TFT was changed according to the irradiation energy of the IPL. This

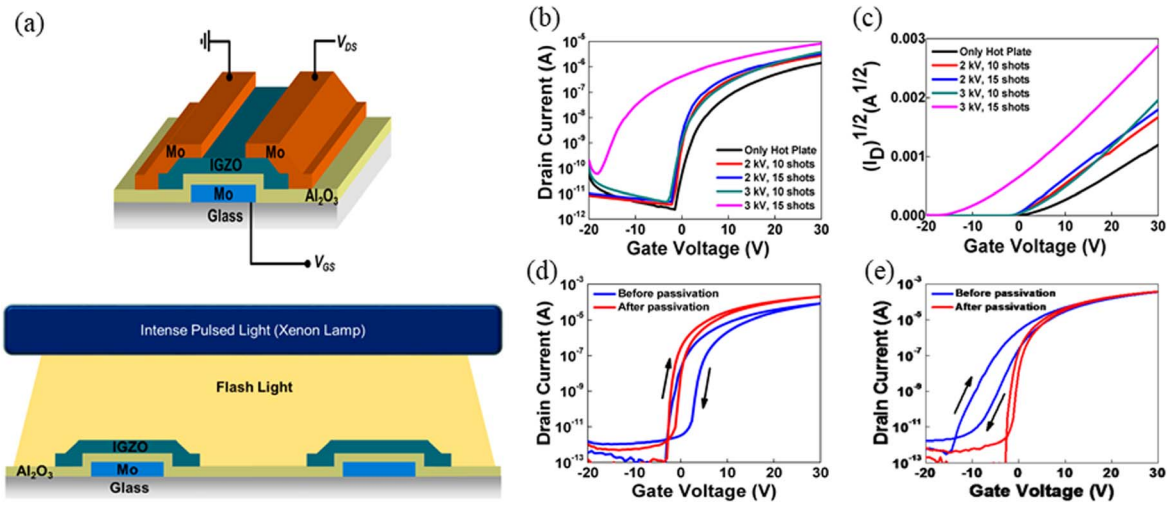

Figure 3. IPL treated IGZO-based thin-film transistors on Si wafer: (a) inverted-staggered TFT structure and IPL annealing system, (b) drain current versus gate voltage plots (logarithmic scale), (c) the square root of drain current versus gate bias transfer curves in comparison with thermal annealing, transfer curves before and after passivation with IPL treatment at (d) 3 kV, pulse time of 1 ms, 15 pulses, and (e) 3 kV, pulse time of 2 ms, 10 pulses. Reproduced from [21]. CC BY 4.0.

could be due to the residual presence of organic ligands in molecular precursors that were not completely removed under conditions of low energy irradiation. However, as the irradiation energy of the IPL increases, the device begins to exhibit a gate bias response. The optimized IPL pulse condition was found to be 10 pulses with a pulse time of 10 ms and a off time span of 10 ms. The voltage applied to the xenon lamp was 430 V, and the total irradiation energy was about 100 J cm^{-2}. The performance of the IPL annealed IGZO TFT was compared with the previously reported thermal annealing for 1 h at 500 °C. The mobility increased by 9.9 times, the on/off current ratio increased by 10^3 times, the threshold voltage decreased from 10 to −12 V, and the subthreshold swing decreased by 0.36 times. As a result, IPL annealed IGZO TFT exhibited excellent performance comparable to thermally annealed IGZO TFT.

Metal oxide TFT manufactured on transparent glass rather than SiO_2/Si wafers require a additional light absorption layer to anneal the metal oxide thin film. Alternatively, a metal gate pattern was used as the light absorbing layer in IGZO TFT on glass substrates [20]. They used a thermocouple thermometer to monitor the temperature of the substrate floor while the IPL was irradiated. Compared to light transmitting glass, Cr gate patterned glass exhibits ∼250 °C higher temperature. Therefore, IPL light annealing requires one of the following conditions: (i) the layer to be sintered must be capable of absorbing visible light, (ii) there must be additional neighboring layer capable of absorbing light, (iii) ultra high energy IPL irradiation should be possible in the absence of a layer capable of absorbing light. They confirmed that IPL irradiation immediately generated sufficient thermal energy to promote the complete conversion of the precursor into an IGZO metal oxide thin film. The optimal condition of IPL annealing was set to applied voltage of 2000 V, pulse time of 15 ms, frequency of 1 Hz and 40 pulses. IGZO TFT with thermal and deep UV (DUV) annealing exhibit field-effect mobilities of 1.8 and 2.2 $cm^2\ V^{-1}{\cdot}s^{-1}$, respectively. Despite a very short annealing time (40 s), IPL annealed IGZO TFTs exhibited field-effect mobility as high as 10.89 $cm^2\ V^{-1}{\cdot}s^{-1}$, virtually no hysteresis, low gate leakage current, and high on/off current ratio of $>10^8$. IPL annealed IGZO TFT exhibited superior electrical properties than conventional thermal and DUV annealed IGZO TFT. SiO_2/Si wafer and the Mo gate pattern on glass substrate were compared to investigate the IPL irradiation according to the substrate (figure 3(a)) [21]. The SiO_2/Si wafer showed conductive transfer characteristics under the conditions of 638 mJ cm^{-2} (3 kV, 2 ms), 15 pulse, but the Mo gate pattern on glass substrate showed conductive transfer characteristics at 323 mJ cm^{-2} (3 kV, 1 ms), 15 pulse, and 638 mJ cm^{-2} (3 kV, 2 ms), 10 pulse. They report on the effects of an IPL rapid annealing process and back-channel passivation in solution-treated IGZO TFT (figures 3(b)–(c)). Generally, metal oxide TFT can be degraded by the adsorption of oxygen or water molecules on the back-channel surface of metal oxide. The back-channel surface of the IGZO channel layer was protected with photosensitive polyimide. Passivated IGZO TFT increased field-effect mobility by 1.41 times and subthreshold swing decreased by 0.32 times compared to that without passivation. Compared with the IGZO TFT fabricated on a Si wafer, the mobility increased 54 times. As a result, it was confirmed that the electrical properties, stability, and uniformity of IGZO TFT arrays can be dramatically improved by using an appropriate back-channel passivation layer (figures 3(d)–(e)). Also, temperature in top surface and bottom surface of the In_2O_3 TFT structure was analyzed through simulation during light pulses [22]. The Al gate pattern of In_2O_3 TFT is used as the light absorption layer. The simulation results show that the temperature of top surface of the stack increases by ∼1000 °C and decreases below ∼200 °C within 6 ms according to a single light pulse with 5 J cm^{-2} and 500 μs. On the other hand, the bottom surface keeps the temperature of the substrate close to room temperature. Applying 20 pulses to this device further increases the temperature of the

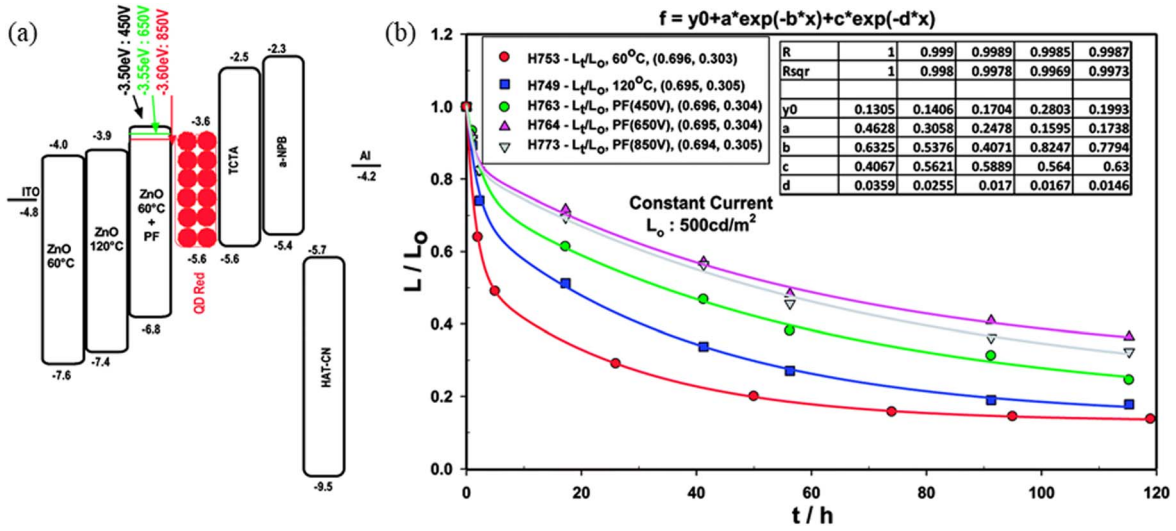

R	1	0.999	0.9989	0.9985	0.9987
Rsqr	1	0.998	0.9978	0.9969	0.9973
y0	0.1305	0.1406	0.1704	0.2803	0.1993
a	0.4628	0.3058	0.2478	0.1595	0.1738
b	0.6325	0.5376	0.4071	0.8247	0.7794
c	0.4067	0.5621	0.5889	0.564	0.63
d	0.0359	0.0255	0.017	0.0167	0.0146

Figure 4. IPL annealing of ZnO electron injection layer in CdSe/ZnS Q-dot LED: (a) energy level diagram, (b) luminance decaying curves in QLED employing ZnO (60 °C), ZnO (120 °C), ZnO (60 °C) + IPL (450 V), ZnO (60 °C) + IPL (650 V) and ZnO (60 °C) + IPL (850 V). Reproduced from [67]. CC BY 4.0.

top surface to ∼1200 °C. However, the bottom surface increases to ∼300 °C. The temperature increase at the bottom surface can in principle be reduced to significantly lower values by using substrate materials with low thermal conductivity (e.g. plastic or paper). As a result, the mobility of IPL annealed In_2O_3 was 6 $cm^2\ V^{-1}{\cdot}s^{-1}$, and that of IPL annealed In_2O_3/zinc oxide (ZnO) was 36 $cm^2\ V^{-1}{\cdot}s^{-1}$. The performance level represents a similar level of performance to that of processing for 1 h at 250 °C.

Nontransparent electrode was used as a light absorbing layer in TFT to accommodate most energy of IPL. However, in some cases such as LED or solar cells, there is metal oxide layer on the transparent electrode. The metal oxide was used as an electron injection layer (EIL) or an electron transport layer (ETL) rather than an active layer. In this case, IPL annealing can control the valence-conduction band level of EIL or ETL [67, 68]. Quantum dot LED (QLED) was manufactured using ZnO as an EIL and the performance of ZnO by IPL annealing was compared (figure 4(a)) [67]. ZnO film was coated on transparent ITO glass and then IPL-annealed. The conduction band level was changed according to the energy of the IPL, which was changed to 3.5, 3.55 and 3.6 eV under the conditions of 22.6 J cm^{-2} (450 V, 1.5 ms, 5 pulse), 37.8 J cm^{-2} (650 V, 1.5 ms, 3 pulse) and 23.6 J cm^{-2} (850 V, 1.5 ms, 2 pulse), respectively. ZnO device annealed by IPL at the condition of 23.6 J cm^{-2} with drying at 60 °C had the same turn-on voltage of 2.2 V as that of ZnO deivce thermally annealed at 120 °C for 30 min at vacuum. Moreover, the current efficiency and power efficiency increased with the irradiation energy of the IPL and were significantly higher than the devices annealed at 120 °C at all luminance levels tested. They showed that the IPL annealed ZnO devices exhibit significantly higher efficiencies and longer lifetimes than the same devices fabricated from thermally annealed ZnO (figure 4(b)). Also, solar cells were fabricated using SnO_2 as ETL, and presented a fast, low temperature solution-based method through IPL annealing [68]. SnO_2 was coated on transparent fluorine doped tin oxide (FTO) coated glass and IPL annealed. Investigation of precursor solutions and photon annealing conditions have shown to form high-quality nanocrystalline SnO_2 films under condition of 46 J cm^{-2} and 20 ms with a $SnCl_4$ concentration of 0.1 M. This enables perovskite solar cells with low hysteresis and high-power conversion efficiencies exceeding 15%.

Eom *et al* analyzed nitrogen-related chemical bonds considering the predominant use of nitrate precursors in solution process [69]. Through the curve of the N 1s peak obtained by x-ray photoelectron spectroscopy (XPS) and the 5 sub-peaks, it was confirmed that the hydroxides and nitrates were transformed into a network of oxides and nitrides between 14 s and 16 s. If the irradiation time is further extended, nitrogen is released from the sol-gel reaction and diffuses into the oxygen-deficient site or high concentrations of nitrogen-occupying vacancies (N_O), creating double nitrogen-occupying defects ($(N_2)_O$) as shown in figure 5(a). This results in a sharp increase in carrier concentration and off current. They believe that XPS analysis of the N 1s peaks reveals the presence of oxygen vacancies-related nitrogen defects and their evolution with annealing time, which may be responsible for increased carrier concentration (figures 5(b)–(g)). As a result, IGZO TFT with the best performance under the condition of irradiation for 16 s was realized.

Since the metal has a low heat treatment temperature and a high absorbance, an effective IPL process is possible for metals [54, 70–72]. However, since metal oxide requires a high-temperature process, a relatively long process time of ∼10 s is required even by IPL. The efficient annealing of metal oxides has been studied. IPL annealing was split into multiple steps and compared to one step [73]. It was confirmed that In_2O_3 was completely converted into an oxidized film within 30 s. The temperature at the back side of the substrate according to the irradiation time was confirmed through experiments and simulations. The temperature of the back side increased sharply up to 20 s and then gradually

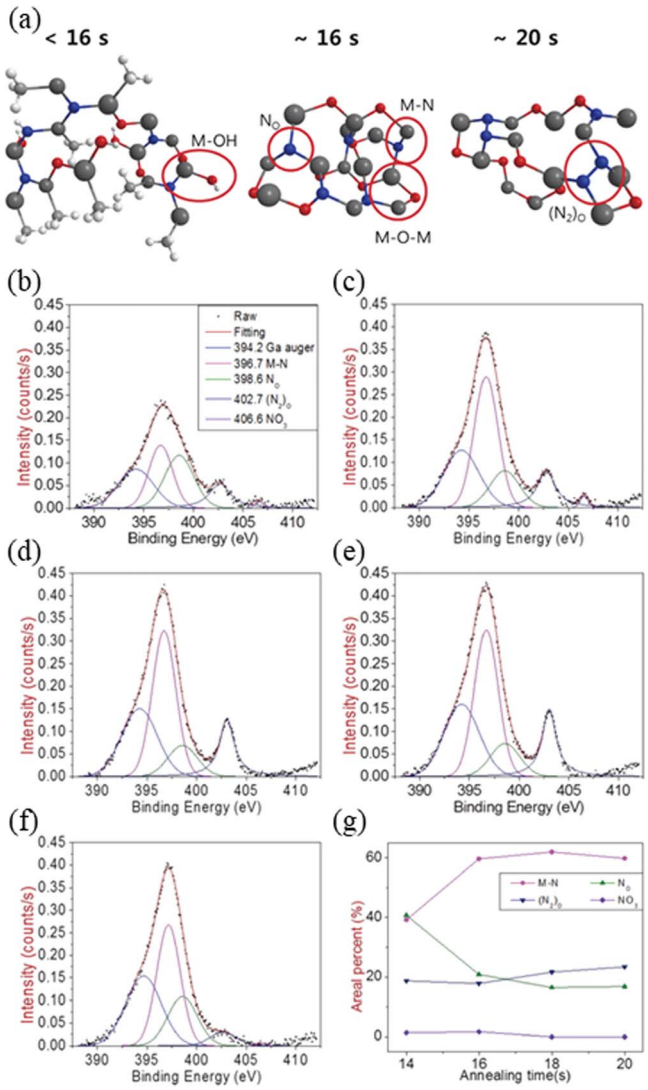

Figure 5. The effect of nitrogen in IPL treated IGZO TFTs: (a) evolution of chemical structure change with IPL irradiation, N 1s peak obtained from XPL analysis with IPL annealing for different time: (b) 14, (c) 16, (d) 18, and (e) 20 s, and (f) the 350 °C thermal annealing. (g) The areal percentage variation of the M–N, N_O, $(N_2)_O$, and NO_3 peaks with IPL annealing time. Reproduced from [69]. © IOP Publishing Ltd. All rights reserved.

increased from 20 to 40 s under condition of 207 J/pulse and 15 Hz. Then, it was kept constant at about 350 °C from 40 s. In_2O_3 TFT implemented in one step process showed the best performance of the device processed in 120 s. However, the substrate exhibits high temperatures. They divided the time into 10 s increments to avoid temperature rise of the substrate. As a result, it showed the best performance under the conditions of 10 s and 3 times. Compared to the result of 120 s, the mobility decreased about 4 times, but the on/off ratio increased about 500 times. It was also able to prevent the temperature rise of the substrate. In addition, the heat treatment effect could be improved by changing the near-infrared (NIR) drying-IPL annealing process to a NIR and DUV drying-IPL annealing process as shown in figure 6(a) [74]. The DUV drying process can have the effect that the bonding of Ga and oxygen formed thereby prevents excessive carrier generation in the IGZO due to oxygen separation during IPL annealing (figure 6(b)). During the drying phase, DUV can control the separation of oxygen and keep the carriers at an appropriate level. After that, high mobility and high on/off ratio can be achieved through IPL annealing (figures 6(c)–(f)). This IPL method is effective for annealing semiconductor materials based on indium and gallium. It has been demonstrated that the use of DUV in the drying phase promotes the bonding of metals to oxygen, particularly gallium to oxygen by XPS analysis. Metal oxide bonding distribution analysis allowed us to control the bonding state of metal and oxygen in IGZO with or without DUV, and this process affected the TFT performance improvement.

2.2. Vacuum deposited thin films

Metal oxide thin films deposited by vapor deposition techniques are discussed for IPL annealing in this section. The metal oxide thin films is formed by various deposition techniques such as direct current (DC) sputtering [75], DC reactive sputtering [76], radio-frequency (RF) sputtering [77], reactive thermal evaporation [78], electron beam evaporation [79], pulsed laser deposition [80], and atomic layer deposition (ALD) [81]. Such thin films usually have residual stress due to the lattice mismatch and the difference in thermal expansion coefficient between thin film and the substrate. Therefore, annealing process is required to relieve the residual stress and/or improve the crystallinity of the thin film [82]. However, the thermal annealing process, where thin films are subjected to annealing chamber, has the disadvantage of damaging the interface between thin film and the substrate [83]. Rapid annealing such as IPL annealing was proposed to address this issue.

First, IPL annealing of semiconducting materials applied to TFT was investigated. Zinc oxynitride (ZnON) was deposited on SiO_2/Si wafer using a DC reactive sputtering and investigated the electrical characteristics of TFT according to IPL irradiation energy from 30 to 50 J cm^{-2} (figure 7(a)) [23]. As the IPL irradiation energy increased, the carrier concentration in the thin film decreased and the electrical characteristics of the device such as mobility, subthreshold swing, hysteresis, and bias stability decreased (figure 7(b)–(c)). The cause of the decrease in electrical characteristics according to the increase of IPL irradiation energy is considered to be (i) change in anion atom concentration, (ii) change in oxygen-related bond state, and (iii) change in nitrogen-related bond. The composition of the ZnON thin film, metal-oxygen bonding, and oxygen depletion did not change significantly after IPL irradiation. However, the ratio of Zn_xN_y and N–N bonds increased in the XPS N 1s spectrum. It can be concluded that the nitrogen-related bonding state in the ZnON TFT has a great influence on the properties of the TFT device. Also, Nitrogenated a-IGZO (a-IGZO:N) thin film was deposited on SiO_2/Si wafer using DC sputtering followed by an IPL annealing [24]. A preheating step using a plate-heater was conducted to improve the efficiency of the IPL annealing process. The simulations involving thermal conduction and radiation were performed to

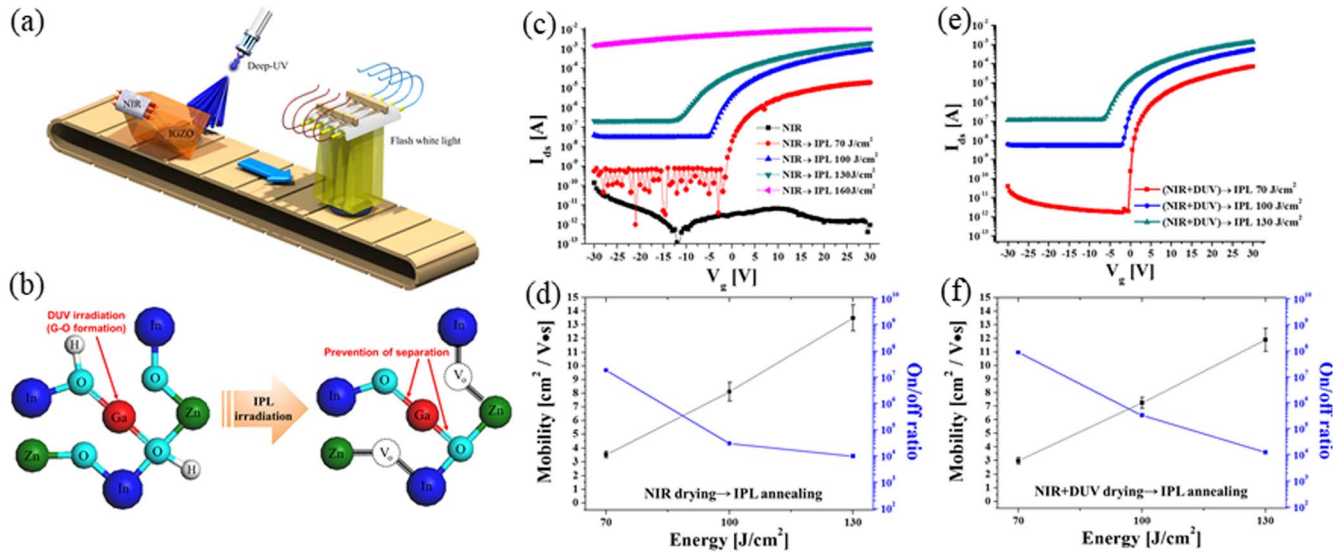

Figure 6. IPL annealing of IGZO TFTs with precedent DUV treatment: (a) schematics, (b) illustration of metal−oxide bond consolidation by gallium−oxide bond activation by DUV irradiation, (c) electrical transfer properties and (d) on/off ratio and mobility of IPL annealed IGZO-based TFTs, (e) transfer properties and (f) on/off ratio and mobility of IGZO-based TFTs annealed using IPL with DUV. Reprinted with permission from [74]. Copyright (2019) American Chemical Society.

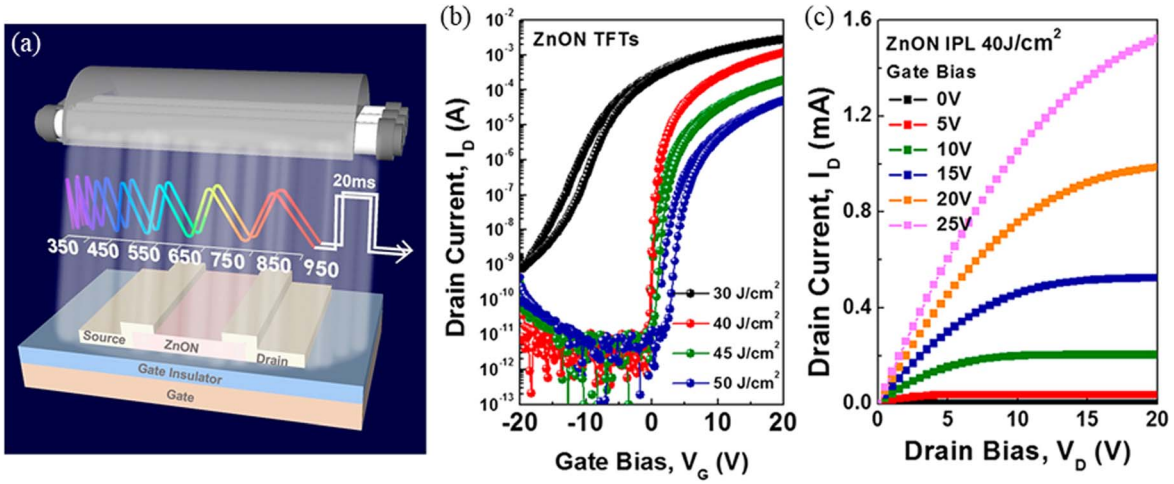

Figure 7. ZnON TFTs by IPL annealing process: (a) schematic of the IPL process, (b) transfer curves with different irradiation energies, (c) output characteristics with irradiation energy of 40 J cm^{-2}. Reprinted with permission from [23]. Copyright (2019) American Chemical Society.

predict the temperature of the substrate. It was confirmed that the thin film instantaneously experienced over 700 °C by the IPL irradiation energy. The effects of IPL annealing were compared with the results from thermal annealing at 100 to 700 °C for 1 h. IPL-annealed a-IGZO:N TFT under condition of 4.8 kV and 1.2 ms on plate-heater of 300 °C had mobility of 4.27 cm^2 $V^{-1}{\cdot}s^{-1}$, threshold voltage of 4.2 V, and on/off current ratio of 8.45 × 10^7. This was similar to the results of thermal annealing at 500 °C for 1 h.

IPL post-treatment was also applied in transparent conducting materials used in optoelectronic devices such as organic LED or photovoltaics. A transparent electrode such as ITO mainly uses a transparent substrate for optical transparency. Since normal IPL irradiation has little effect on annealing, an additional process such as inserting a polyimide (PI) layer or using a back-reflector was adopted. ITO thin film deposited by the RF magnetron sputtering on PI thin film of 16 μm in thickness was annealed using the IPL process [84]. ITO was deposited on glass coated with PI thin film of 16 μm in thickness (figure 8(a)). To improve the electrical and optical properties of the ITO thin film, IPL was applied under various conditions and compared with thermal annealing for 1 h. The x-ray diffraction (XRD) pattern showed that the microstructure of the ITO thin film was converted from an amorphous to a crystalline phase by the IPL process. In addition, the surface roughness was greatly increased and became comparable to that observed in thermal annealing process. The resistivity of the ITO thin film was reduced by about 50% and 75% through IPL and thermal annealing processes, respectively (figures 8(b)–(c)), compared to as-deposited ITO film. On the other hand, the light transmittance increased slightly in the visible light region (figure 8(d)). As

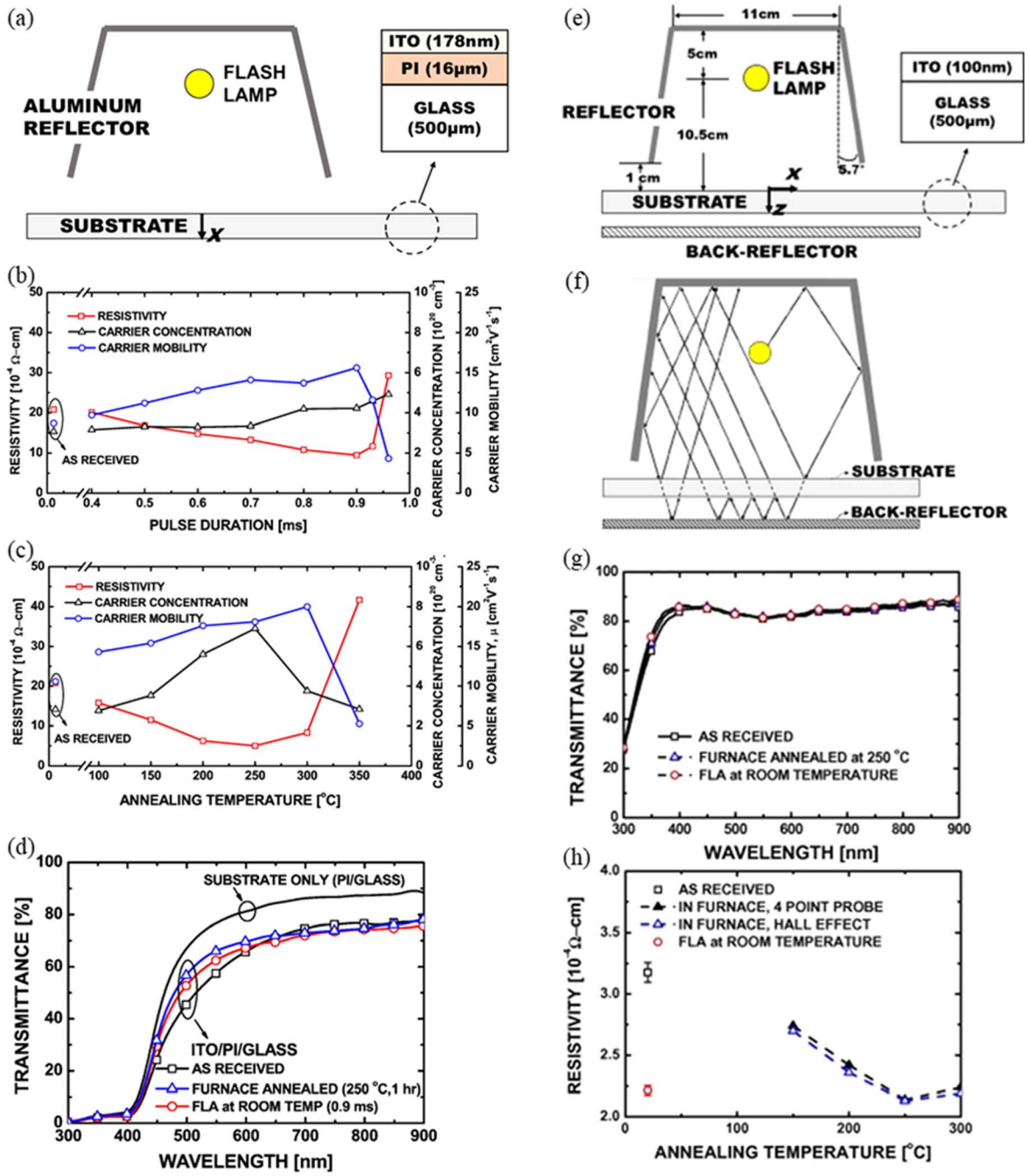

Figure 8. IPL annealing employing absorption layer and back-reflector for vacuum deposited ITO on glass substrate: (a) schematic of IPL annealing system using additionally coated PI, electrical resistivity, carrier concentration, and carrier mobility of ITO thin films (b) IPL annealed and (c) thermally annealed for 1 h, (d) comparison of spectral transmittances of ITO thin films. Reprinted from [84], copyright (2017), with permission from Elsevier. Schematic of (e) IPL annealing system using back-reflector and (f) ray-tracing emitted from the lamp, comparison of (g) spectral transmittances and (h) resistivity of the ITO thin films. Reprinted from [85], Copyright (2015), with permission from Elsevier.

the pulse time of the IPL process is increased, the temperature of the substrate exceeds the crystallization point of the ITO material to obtain high crystallinity of ITO. However, at pulse times longer than 0.9 ms, where the lowest resistivity was found, the severely damaged microstructure was observed. It was due to the difference in thermal expansion of ITO and PI leading to fracture of ITO film. The introduction of a back-reflector for transparent ITO glass can improve the annealing effect [85]. ITO was deposited directly on the glass substrate without any intervening layer by RF magnetron sputtering. A back-reflector was utilized below the substrate during IPL annealing as shown in figure 8(e). This reflects the IPL that has passed through the ITO glass and causes it to act on the ITO glass again. (figure 8(f)). The total amount of IPL applied to the ITO glass is increased by the reflected IPL. According to ray-tracing calculations, the absorbed energy is 2.8 times higher when the back-reflector is used. In the visible light region, the transmittance was still high without any change,

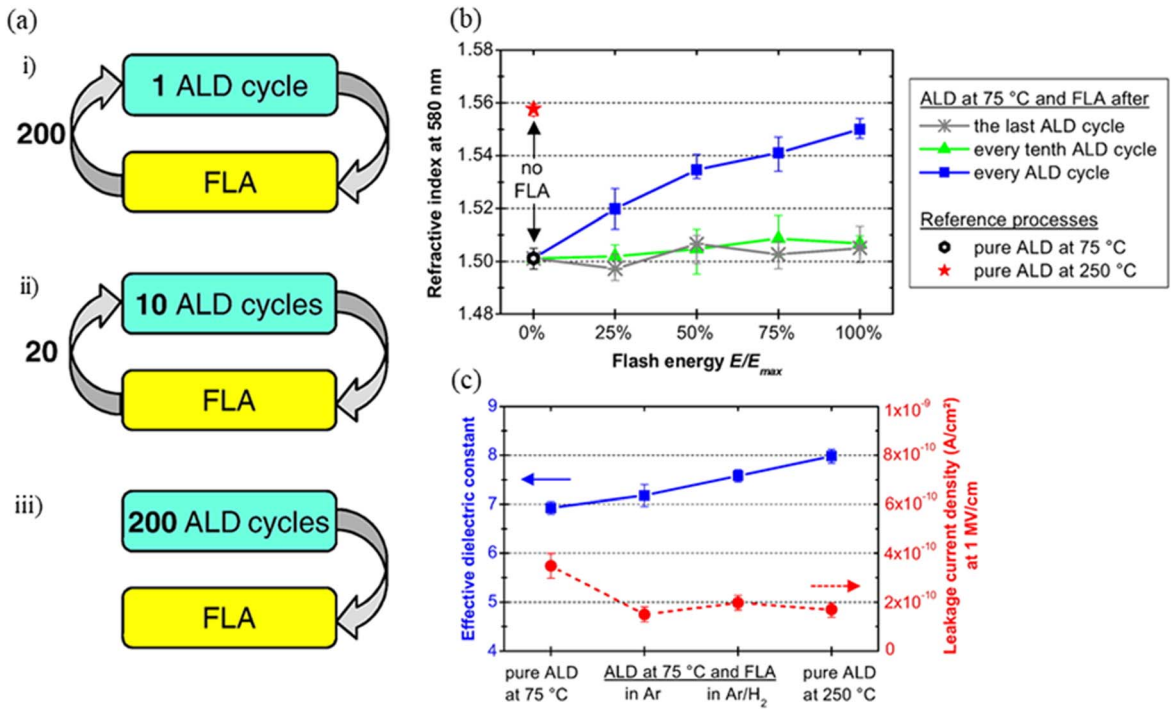

Figure 9. IPL annealing of Al_2O_3 films grown using atomic layer deposition (ALD): (a) illustration of process configuration, (b) refractive index of Al_2O_3 films grown at 75 °C and treated with *in situ* IPL annealing in different process configurations, (c) comparison of effective dielectric constant and leakage current density at an electric field of 1 MV cm^{-1}. Reprinted from [26], copyright (2017), with permission from Elsevier.

but the resistivity was decreased by 30% (figures 8(g) and (h)) due presumably to increase in carrier mobility. The same effect was obtained at thermal annealing at 250 °C for 1 h.

IPL annealing of dielectric materials was improved by using preheat processes or irradiating IPL during deposition. The effect of IPL annealing of hafnium-zirconium-oxide ($Hf_xZr_{1-x}O_2$, HZO) deposited on a Si wafer using plasma enhanced atomic layer deposition was compared with rapid thermal annealing (RTA) process for ferroelectric application [25]. Unlike thermal annealing, which generally raises and lowers the temperature slowly and gradually, the RTA process is a process in which the temperature change is rapid [86–88]. IPL annealing was conducted with 70 J cm^{-2} for 20 ms preceded by a preheat at 375 °C for 120 s, and the ferroelectric properties of IPL annealed HZO was similar to those of HZO annealed by RTA at 650 °C for 300 s. It was also demonstrated that ferroelectric behavior appears at $x = 0.57$ ($Hf_{0.57}Zr_{0.43}O_2$) in IPL annealing. A study of performing IPL annealing during deposition in the ALD cycle based on Al_2O_3 was also reported [26]. Al_2O_3 thin films formed by low temperature ALD have low density. IPL annealing has been proposed to increase the density of Al_2O_3 thin films with short-term heat treatment. ALD was deposited in a total of 200 cycles at 75 °C. IPL annealing was performed after the last ALD cycle, every tenth ALD cycle and every ALD cycle as shown in figure 9(a). Among them, the Al_2O_3 thin film annealed after every ALD cycle had highest density, 10% increased value (figure 9(b)). As the density increases during the densification process, the thickness generally decreases. However, both density and thickness of ALD-grown Al2O3 increased, which is not considered densification but promotion of film growth. The IPL irradiation energy directly affects the surface chemistry, such as reduction of the surface density of −OH− groups, desorption of physically adsorbed H_2O from the surface, or removal of residual carbon contamination. As a result, the mass gain per cycle is increased by 25%, similar to Al_2O_3 films processed by ALD at 250 °C without IPL treatment. IPL irradiation energy promotes the growth of Al_2O_3 at the expense of the aluminum hydroxide component. The IPL treatment every ALD cycle yielded increased refractive index, increased dielectric constant, and decreased leakage current (figure 9(c)). Moreover, it did not affect the structure of the thin film, and the film remained amorphous and smooth.

3. IPL post-treatment of metal oxide nanostructures

Metal oxide nanostructures are currently of tremendous interest to scientists and engineers because of their potential for new applications ranging from catalysts, sensors, and microelectronics to energy conversion devices including solar and fuel cells. Zero-dimensional (0D) metal oxide nanostructures such as nanoparticles [89–91] are common materials and have been mainly studied in nanotechnology. 0D metal oxide nanomaterials are currently widely used in many fields such as catalysts [92], sensors [93], transparent conductive films [94], electro-optical [95] and electro-chromic [96] devices. Not only 0D, but also various nanostructures of 1D, 2D and 3D such as nanowires [97], nanorods [98], nanobelts

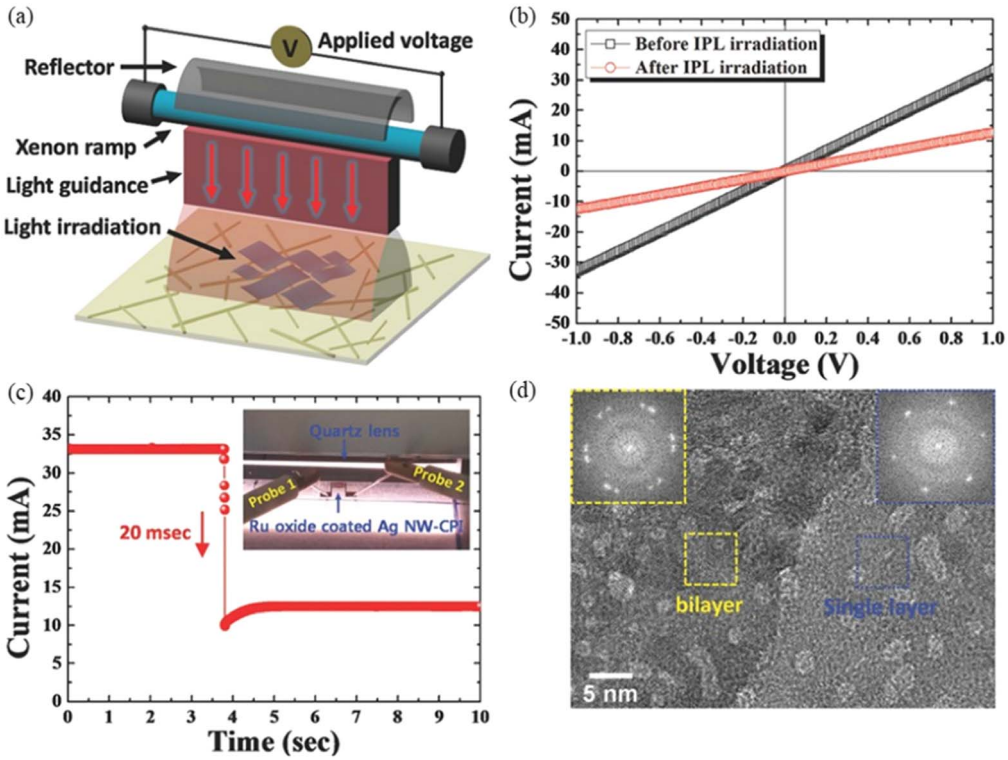

Figure 10. IPL treatment of RuO_2 nanosheet gas sensors: (a) schematic illustration of IPL sintering, (b) current–voltage characteristic before and after IPL sintering, (c) *in situ* current transition during the IPL sintering, (d) TEM analysis of the porous RuO_2 nanosheets [109]. John Wiley & Sons. © 2017 WILEY-VCH Verlag GmbH & Co. KGaA, Weinheim.

[99], nanosheets [100], nanoflowers [101] have been studied. Metal oxide nanostructures are characterized by their intrinsic properties and large surface area-to-volume ratio, which enhance their usefulness in new applications [102]. In addition, nanostructures have the advantage of lower heat treatment temperature compared to bulk materials [103, 104]. In this section, IPL sintering and IPL annealing of metal oxide nanostructures are reviewed. In particular, copper oxide (CuO) nanostructures showed both sintering and annealing characteristics by IPL and were separately reviewed.

3.1. Sintering of metal oxide nanostructures

Metal oxide nanostructures with a scale of less than 100 nm can be fabricated by various synthetic methods such as hydrothermal [105], solvothermal [106], and sol-gel [107] method. Because of the interesting properties of nanostructures (mechanical, optical and electrical), the material has been studied extensively. These properties are related to the high density of grain boundaries due to the nanoscale structure. Many researchers have improved the properties of nanostructures by using a sintering process to control grain boundaries. By sintering, the nanostructures grow grains. The growth of grains can improve mechanical, optical, and electrical properties, and solve the problem of metastable phase in ultrafine nanostructures. However, excessive grain growth may cause the inherent properties of nanoscale to disappear. In this section, IPL sintering of solution process-based nanostructures was reviewed.

Ruthenium oxide ($RuO_2{\cdot}xH_2O$) nanoparticles with size of 100 nm were sintered using IPL, compared with thermal sintering, and exploited for application in supercapacitors [108, 109]. The specific capacitance of the supercapacitors was optimized by IPL irradiation on $RuO_2{\cdot}xH_2O$ at 2.04 J cm^{-2} (1.5 ms of pulse time, 10 ms of off time and 2 pulse). The specific capacitance increased by 1.19 times at 10 mV s^{-1} compared to thermally sintered RuO_2 at 150 °C. Compared to the sol-gel derived thin film introduced in 2.1, the nanostructures were sintered even at very low irradiation energies. RuO_2 nanosheets were fabricated and incorporated them into a colorless polyimide film with embedded silver nanowires for application to wearable chemical sensors as shown in figure 10(a). The IPL process reduced the electrical conductivity of RuO_2 nanosheets by 2.65 times (figure 10(b)). The *in situ* current measurement showed that the electrical resistance of RuO_2 nanosheets increased within a time of 20 ms (figure 10(c)) upon a pulse of IPL with 1.15 J cm^{-2}, which is relatively very low energy. The increase in resistance is due to the pores of 5 nm or less generated by the IPL process (figure 10(d)). The formed pores increase the sensing area of the nanosheet, which can detect more gas molecules on the surface.

The IPL process can be combined with other processes to increase its effectiveness. The following is a study that increased the effect of the IPL process through UV pretreatment. DUV irradiation with IPL irradiation process increased the IPL sintering effect of ZnO nanosheets (figure 11(a)) [110]. They applied IPL/DUV-treated ZnO nanosheets as

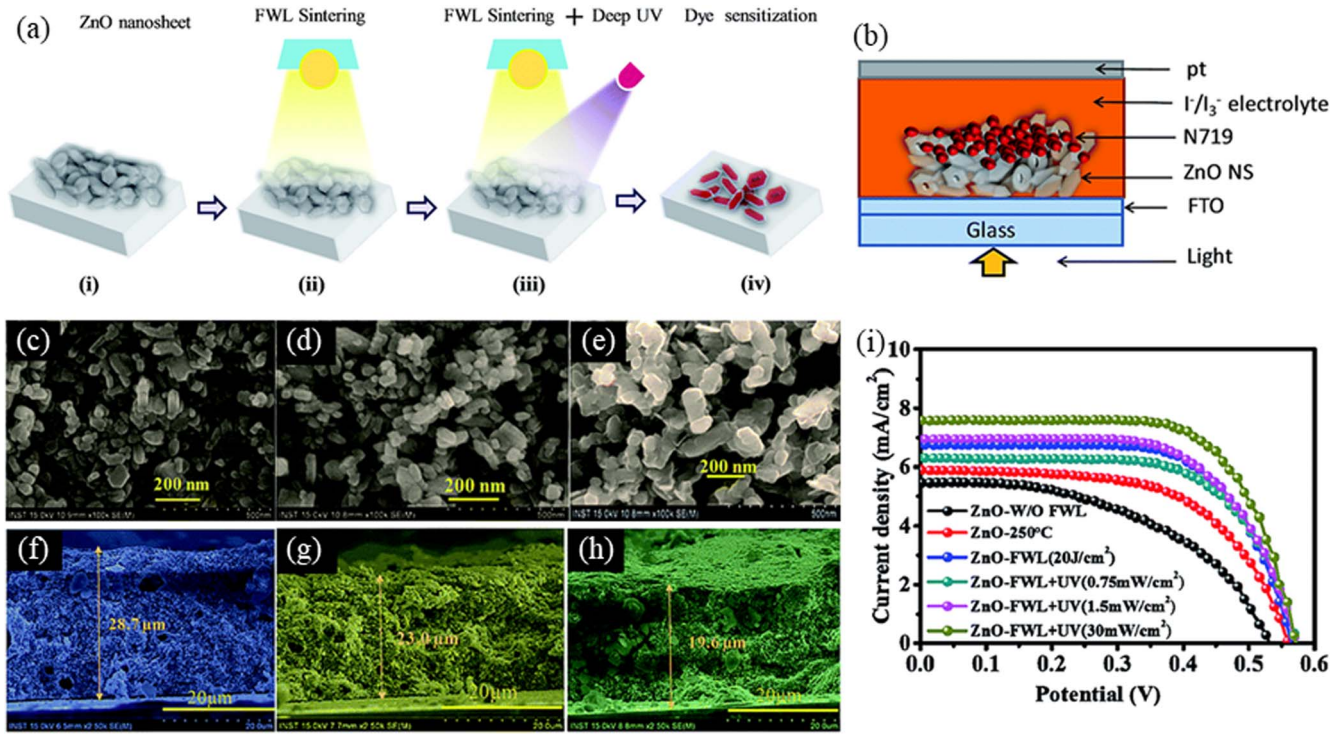

Figure 11. Concurrent DUV and IPL sintering of ZnO nanosheet as photoanode for DSSCs: (a) schematic, (b) structure of DSSCs with FTO/ZnO nanosheets/N 719 dye/electrolyte (iodide/triiodide)/Pt, scanning electron microscope images of (c) ZnO, (d) ZnO with IPL sintering (20 J cm^{-2}) and (e) ZnO with concurrent IPL and DUV (30 mW cm^{-2}), the cross-sectional images (f)–(h) corresponding to (c)–(e), (i) comparison of *J*–*V* curves. Reprinted with permission from [110]. Copyright 2017 Royal Society of Chemistry.

photoanode in DSSC (figure 11(b)). Figures 11(c)–(e) shows SEM images of untreated, DUV-treated, and IPL/DUV-treated the surface of the ZnO nanosheet thin film. The IPL/DUV-treated ZnO nanosheets were grown with larger oxide particles, reducing the grain boundaries as shown in figure 11(e). The increase in particle size decreases the light harvesting efficiency in solar cell because the semiconductor surface is reduced, and the dye adsorption is lowered. However, the reduction of grain boundaries reduces the dangling bonds acting as charge trapping centers, which improves the charge collection efficiency of the photoanode. The cross-section of the ZnO nanosheet thin film was shown in figures 11(f)–(h). After sintering, the thickness of the thin film decreases, which is due to the conversion to a highly crystalline structure. The power conversion efficiency of DUV/IPL-treated ZnO nanosheet (IPL: 20 J cm^{-2}, 20 ms, DUV: wavelength of 180–280 nm, power of 30 mW cm^{-2}) increased to 1.45 times that of thermal sintered ZnO at 150 °C for 30 min, and increased to 1.16 times that of IPL sintered ZnO (figure 11(i)).

On the other hand, a perovskite nanoparticle requires more energy for sintering [111–113]. The general IPL processes do not apply sufficient energy for sintering of perovskite nanoparticle. This could be improved by adding a pretreatment process or a heater. IPL sintered perovskite-structured lanthanum nickel oxide ($LaNiO_3$; LNO) thin films was demonstrated [114]. To prove electrical properties of LNO IPL sintering, the authors performed the IPL process on plate-heater of 500 °C. The XRD pattern on thermal sintering shows that perovskite crystal grow as the temperature increases from 700 °C to 900 °C. However, when the sintering temperature increased, a nickel oxide (NiO) peak appeared in addition to the perovskite crystalline peak. As shown in figure 12(a), the observed NiO peak in the XRD pattern confirmed the phase transition from the perovskite to the Ruddlesden–Popper structure. Figure 12(b) confirms that the sintered material was transformed into $La_4Ni_3O_{10}$ when sintered at 1000 °C and 1100 °C. On the other hand, figure 12(c) shows that IPL IPL sintered LNO thin films have the same perovskite crystallinity irrespective of the energy conditions. It was confirmed that the IPL sintered LNO thin film did not show secondary phase formation and that perovskite crystallinity could be generated through IPL. Its crystallinity was similar compared to thermal sintering. Thermally sintered LNO films at 700 °C for 2 h have a slightly lower resistivity than IPL sintered LNO films at 80 J cm^{-2} (30 ms of pulse time, 80 ms of off time and 6 pulse) as shown in figure 12(d). This result shows that the electrical performance of the LNO film is not low when compared with other literatures. A two-step of IPL irradiation process for lanthanum strontium cobaltite (LSCO) was performed [115]. At the first step, low energy was irradiated to remove residual organic matter, and at the second step, high energy was irradiated for further sintering (figure 12(e)). Due to susceptibility and damage of substrate at the second step, the heating plate was also used to reduce irradiation energy of IPL. The heating plate played a role in compensating the reduced irradiation energy. IPL sintered LSCO at room

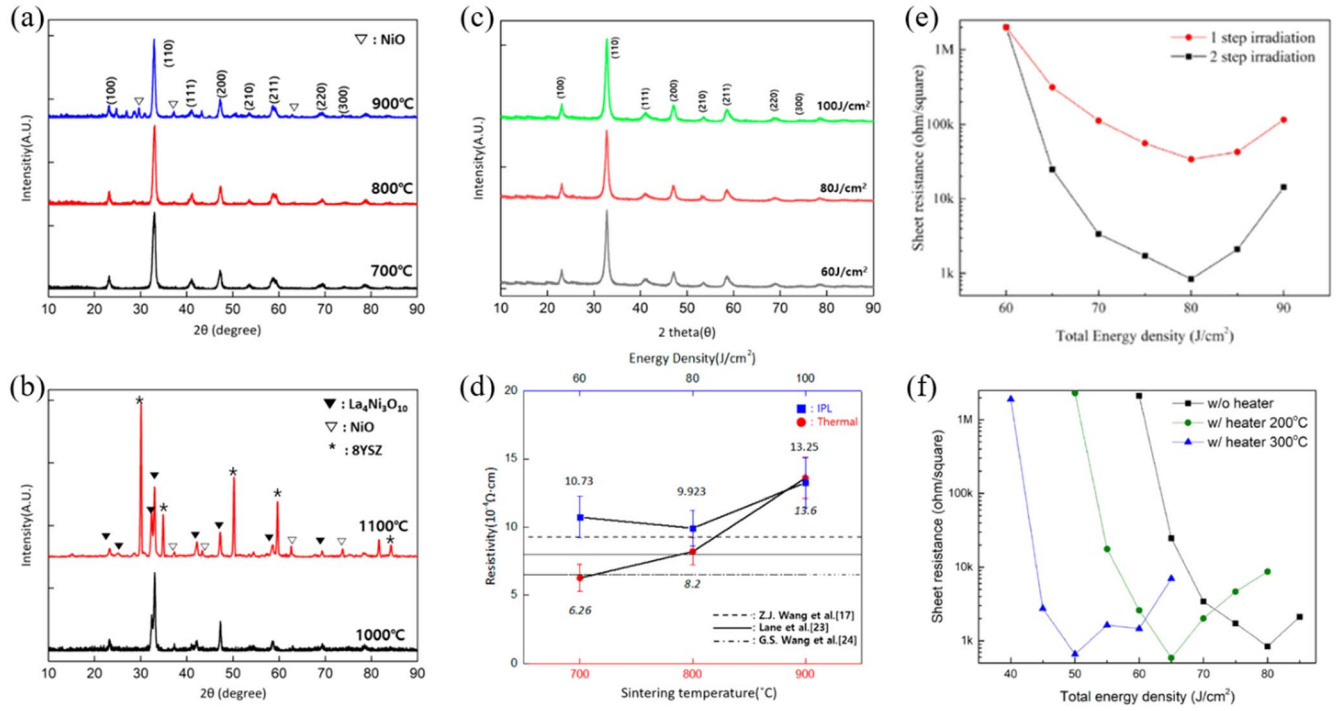

Figure 12. IPL sintering of perovskite nanoparticle film for conductive layers: (a) x-ray diffraction patterns of perovskite LNO thin films thermally sintered at (a) 700, 800, and 900 °C, and (b) Ruddlesden–Popper (RP) structure thermally sintered at 1000 and 1100 °C, and (c) perovskite LNO thin films sintered using IPL at 60, 80 and 100 J cm^{-2}, (d) comparison of resistivity of the sintered LNO films. Reproduced from [114]. CC BY 4.0. Sheet resistance of LSCO film sintered by (e) IPL only and (f) IPL with heater. Reprinted from [115], Copyright (2020), with permission from Elsevier.

temperature without plate-heater required an energy of 80 J cm^{-2}, but IPL sintered LSCO at 300 °C decreased to an energy of 50 J cm^{-2} to reduce the sheet resistance (figure 12(f)).

Since nanostructures have a large surface-to-volume ratio, they require less energy to be sintered or annealed compared to thin film structure. Even in nanostructure incorporated onto transparent substrate, ordinary condition of IPL can treat effectively for device applications such as LEDs. The effect of IPL sintering on ZnO ETL was reported for QLEDs. The authors did the IPL post-treatment not on a single layer of ZnO nanoparticles, but on a multi-layer coated with various materials as shown in figure 13(a) [116]. The XPS spectrum demonstrated that the oxygen vacancy in the ZnO lattice was filled with oxygen by IPL (figure 13(b)). In addition, the Zn^{2+} ions in the lattice were not damaged even after IPL sintering. Figure 13(c) shows the improvement of hole-electron injection balance in quantum dot (QD) emission layer (EML) by IPL sintering. If untreated by IPL, the amount of injected electrons at the interface between the QD EML and the ZnO nanoparticle ETL is greater than the amount of holes injected at the interface between the hole transport layer and the QD EML. This imbalance is resolved by ZnO nanoparticle ETL with reduced electrons due to reduced oxygen vacancy after IPL sintering, as shown in figure 13(d). Besides, after IPL sintering, the properties of QLEDs decreased sharply from the initial state due to the positive aging effect of ZnO nanoparticles ETL. The current density curve was kept constant during the measurement period of 8 d because the oxygen deficiency acting as a trap for ZnO was sufficiently filled with atmospheric oxygen due to the IPL sintering (figure 13(e)–(f)). QLEDs aged sufficiently by IPL retain their luminance and efficiency characteristics. ZnMgO nanoparticles as ETL for QLED were also reported as shown in figure 13(g) [117]. The IPL sintering onto ITO glass (bottom) and Al (top) for sintering of ZnMgO and local annealing of the Al/ZnMgO interface was performed using the transparent substrate characteristics (figure 13(h)). Since the Al pattern is opaque a bit, the Al/ZnMgO interface cannot be directly irradiated by IPL onto the Al side. However, when sintering onto the ITO side, light can pass through the transparent ITO layer to reach the Al/ZnMgO interface. For both methods, the current efficiency increased. Among them, IPL sintering on the Al side showed higher efficiency. The reason is that the heat generated in Al by IPL can be transferred to the interface of Al/ZnMgO, and the Al electrode was more annealed by direct irradiated IPL. The maximum current efficiency of the device irradiated with IPL on the Al side was higher in the optimal condition (figures 13(i)–(j)). After IPL sintering, the maximum current efficiency increased by 1.15 times. EQE improved by 2.7 times and 1.9 times at 100 cd m^{-2} and 1000 cd m^{-2}, respectively (figures 13(k)–(l)). The reduction of electron injection by the formation of AlO_x at the interface of Al/ZnMgO improves the efficiency of the QLED by carrier injection/transport more balanced.

The effect of IPL sintering on vanadium dioxide (VO_2) nanoparticles was studied for thermochromic layers [118]. IPL sintering causes the organic vehicle to evaporate rapidly,

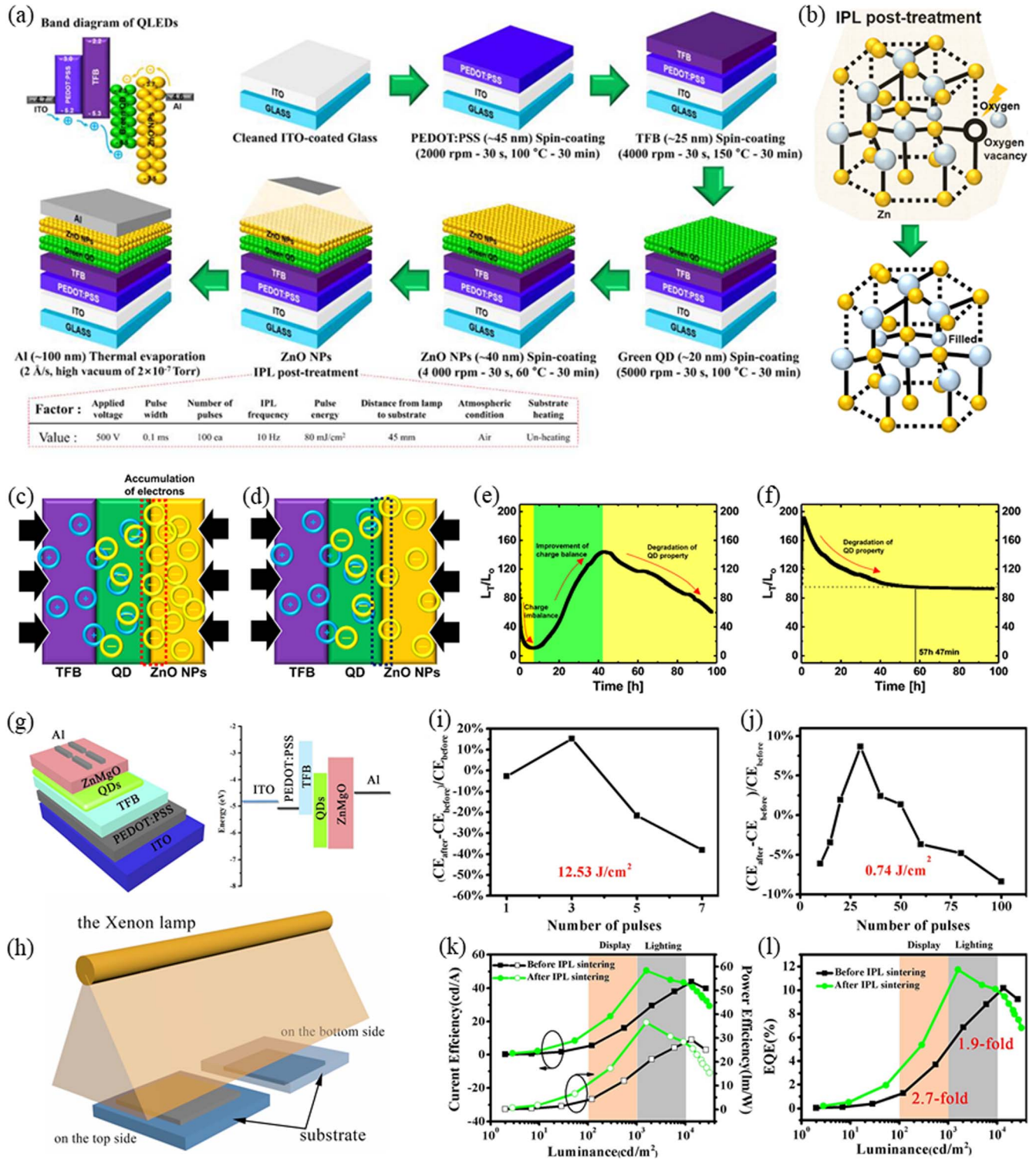

Figure 13. IPL sintering of ZnO and ZnMgO nanoparticles for ETL in QLED application: (a) illustration of band diagram and fabrication process for QLEDs, (b) oxygen vacancy in the ZnO filled with oxygen after IPL sintering, schematics of interfaces structure between TFB, QD, and ZnO NPs (c) without and (d) with IPL sintering, lifetime measurement (e) without and (f) with IPL sintering. Reproduced from [116]. CC BY 4.0. Schematic of (g) structure and band diagram for QLEDs, (h) IPL sintering on the top and bottom side, the maximum current efficiency corresponding to (i) the top and (j) the bottom side, (k) current and power efficiency and (l) EQE with before and after IPL sintering. Reprinted from [117], Copyright (2018), with permission from Elsevier.

resulting in the formation of larger pure VO_2 clusters. Compared with thermal sintering, the crystallinity increased and thermochromic performance of VO_2 nanoparticle-based films were greatly improved. As the number of IPL pulses increased, thinner and denser VO_2 nanoparticle films could be obtained after IPL sintering (figures 14(a)–(d)). Figures 14(e)–(f) shows photographs of VO_2 films thermally sintered on a quartz substrate and sintered by IPL, respectively. The IPL

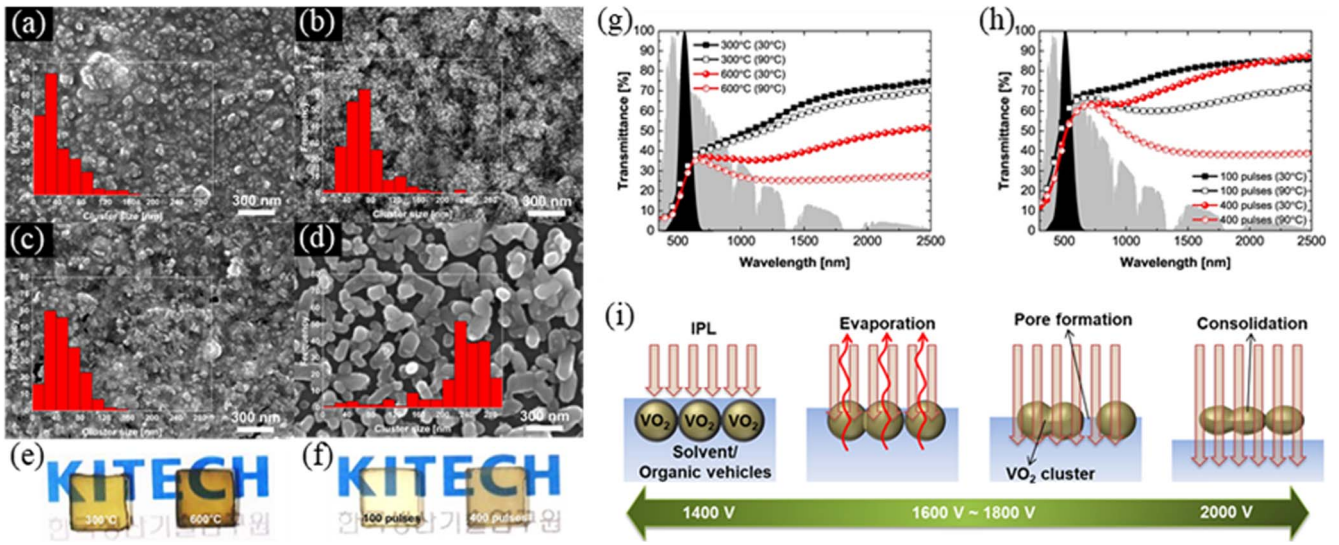

Figure 14. IPL sintering for VO_2 nanoparticles films for thermochromic smart window application: SEM images of VO_2 films after thermal sintering at (a) 300 °C, (b) 600 °C, and after IPL sintering with (c) 100 pulses, (d) 400 pulses, photographs of VO_2 films (e) thermally sintered and (f) IPL sintered, (g), (h) their transmittance spectra. Reprinted from [118], copyright (2019), with permission from Elsevier. (i) schematic illustration of IPL sintering mechanism. Reprinted from [119], copyright (2019), with permission from Elsevier.

sintered VO_2 film was more transparent and visible with a tan color compared to the thermally sintered film. Particularly, the VO_2 film sintered at 400 pulses increased by 2.27, 2.16 and 1.84 times in transmittance at 550 nm, infrared modulation at 2000 nm, and solar modulation efficiencies that of the film thermally annealed at 600 °C for 1 h, respectively (figures 14(g)–(h)). They also studied effect of amount of IPL energy and proposed the sintering mechanism as shown in figure 14(i) [119]. In the film treated at low IPL energy, the VO_2 nanoparticles on the top surface are still covered with organic compounds and solvents. Increasing the IPL causes the formation of pores due to evaporation of the solvent and organic vehicle and exposes the VO_2 clusters on the top surface of the film. At the optimal irradiation energy, the surface roughness is enhanced due to neck growth between VO_2 clusters and mainly transverse strengthening.

3.2. Annealing of metal oxide nanostructures

Annealing of metal oxide nanostructures is a process related to the internal structure of crystals, unlike sintering that control grain boundary. Because the annealing and sintering processes mainly use heat, the effects on nanostructures appear at the same time. Therefore, the process in which the effect is greater among the two processes can be said to be the main process. Annealing causes chemical reactions that change the structure of metal oxide nanostructures to synthesize new materials or induce redox reactions that control oxygen vacancy of materials, and physical reactions that change phases.

Based on the CoO nanostructure, a study has been reported in which the structure of the material is changed by IPL annealing [120–122]. The structure $CoCl_2$ coated on a Nickel-foam (Ni-foam) substrate changed by IPL annealing was investigated [120]. As shown in figures 15(a), (b), under the IPL irradiation 20 J cm^{-2} for 15 ms, the $CoCl_2$ nanocube is transformed into a nanoflake shape for a very short time. IPL-irradiated films exhibit a hierarchical morphology with interconnected nanoflakes with a size of 150–200 nm and a thickness of approximately 10 nm (figure 15(c)). Connected nanoflakes channel had the nano-sized pores (50 nm) that was formed by the instantaneous evaporation of gas molecules within the nanocubes during IPL irradiation. Nanoscale pore channels have the advantage of facilitating the penetration of electrolytes in supercapacitor applications, reducing contact resistance at the electrode/electrolyte interface and facilitating mass/charge transfer. Co/CoO_x core/shell nanoflakes directly on graphite felt (GF) was easily grown using IPL treatment (figure 15(d)) [121]. During the IPL irradiation, $Co(NO_3)_2$ is converted to CoO_x nanoflakes, and the core part of the CoO_x nanoflakes is located very close to the GF substrate, so it is easily reduced to Co carbothermal reaction. (figure 15(e)). However, the part of the shell away from the GF substrate is exposed to the air and remains as CoO_x. The content of CoO_x and Co can be controlled by adjusting the IPL irradiation energy. Increasing the IPL irradiation energy increases the temperature of the GF, causing further reduction of Co_3O_4, CoO, finally to Co. Therefore, as the irradiation energy increases, the relative content of Co compared to CoO_x increases. The core/shell nanoflakes then provide a large reaction area to facilitate OH ion transport due to their three-dimensionally interconnected network structure for energy storage application. Co_3O_4 and Co nanostructures using IPL treatment on carbon fiber paper (CFP)) were reported as shown in figure 15(f) [122]. The $Co(NO_3)_2$ is converted to Co_3O_4, CoO or Co depending on the energy. At the irradiation energy of 10–18 J cm^{-2}, it is converted into Co_3O_4 nanoparticles, and as the irradiation energy increases, Co_3O_4 is reduced, and CoO and Co coexist. At irradiation energy of 26–30 J cm^{-2}, it exists only in the Co state (figure 15(g)). The surface shape according to the IPL energy

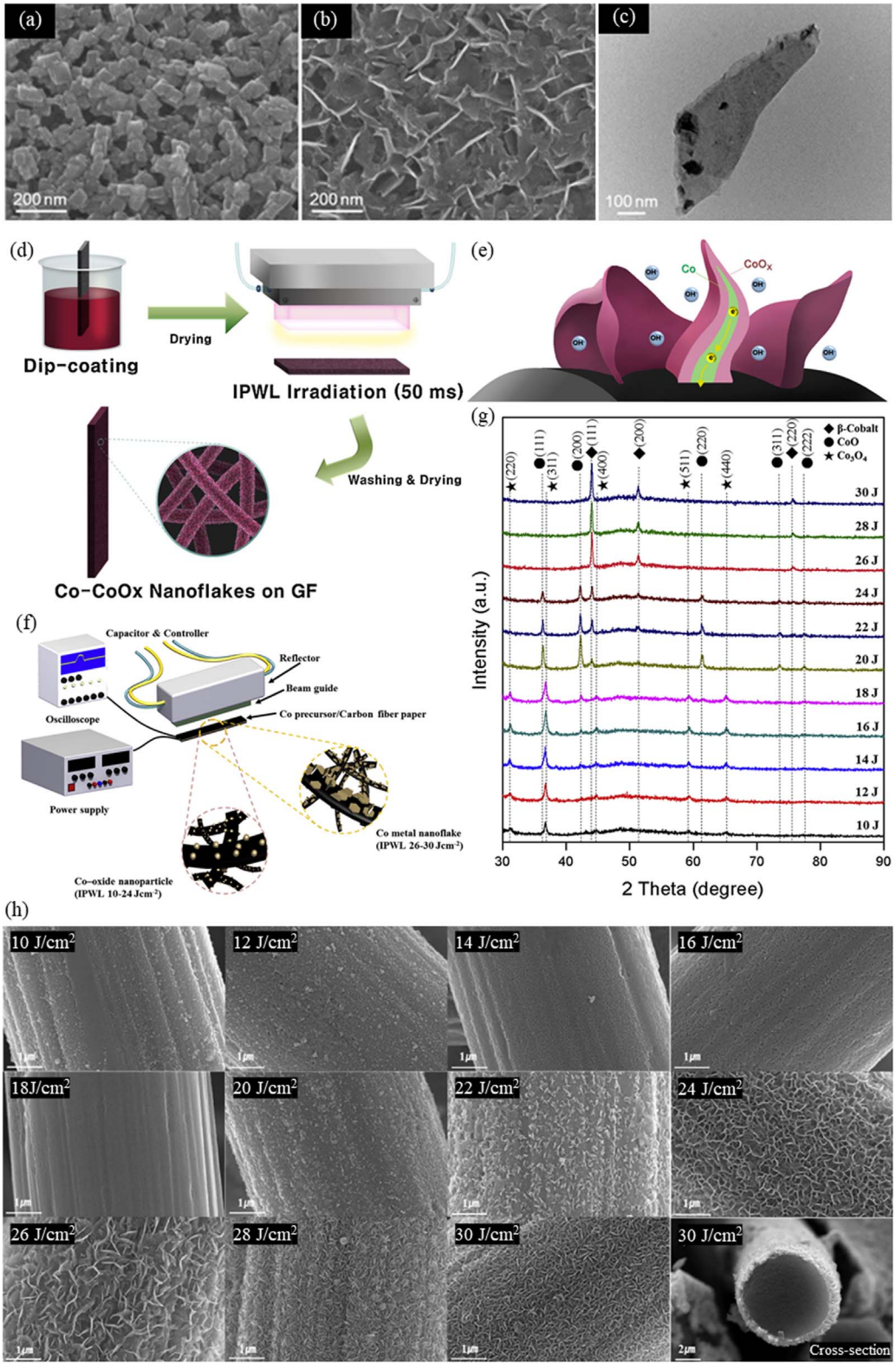

Figure 15. IPL annealing of cobalt oxide for energy storage system: ive $CoO/NiCo_2O_4$ nanoflakes fabricated by IPL annealing: SEM images of (a) cobalt chloride nanocubes and (b) CoO nanoflakes after IPL irradiation, (c) TEM image of CoO nanoflake. Reprinted from [120], copyright (2015), with permission from Elsevier. Analysis of cobalt/cobalt oxide nanoflakes grown on flexible graphite felt and carbon fiber paper via IPL process: (d) schematic of fabrication of Co-CoOx/GF electrode using IPL annealing, (e) detailed view of core/shell structure. Reprinted from [121], Copyright (2017), with permission from Elsevier. (f) Schematics of IPL radiation process for the synthesis of Co metal nanoflakes and Co-oxide nanoparticles on CFP, (g) XRD spectra of the $Co(NO_3)_2$-coated CFP substrates after IPL irradiation with various energy densities, (h) SEM images of $Co(NO_3)_2$-coated CFP substrates after IPL irradiation. Reprinted from [122], copyright (2017), with permission from Elsevier.

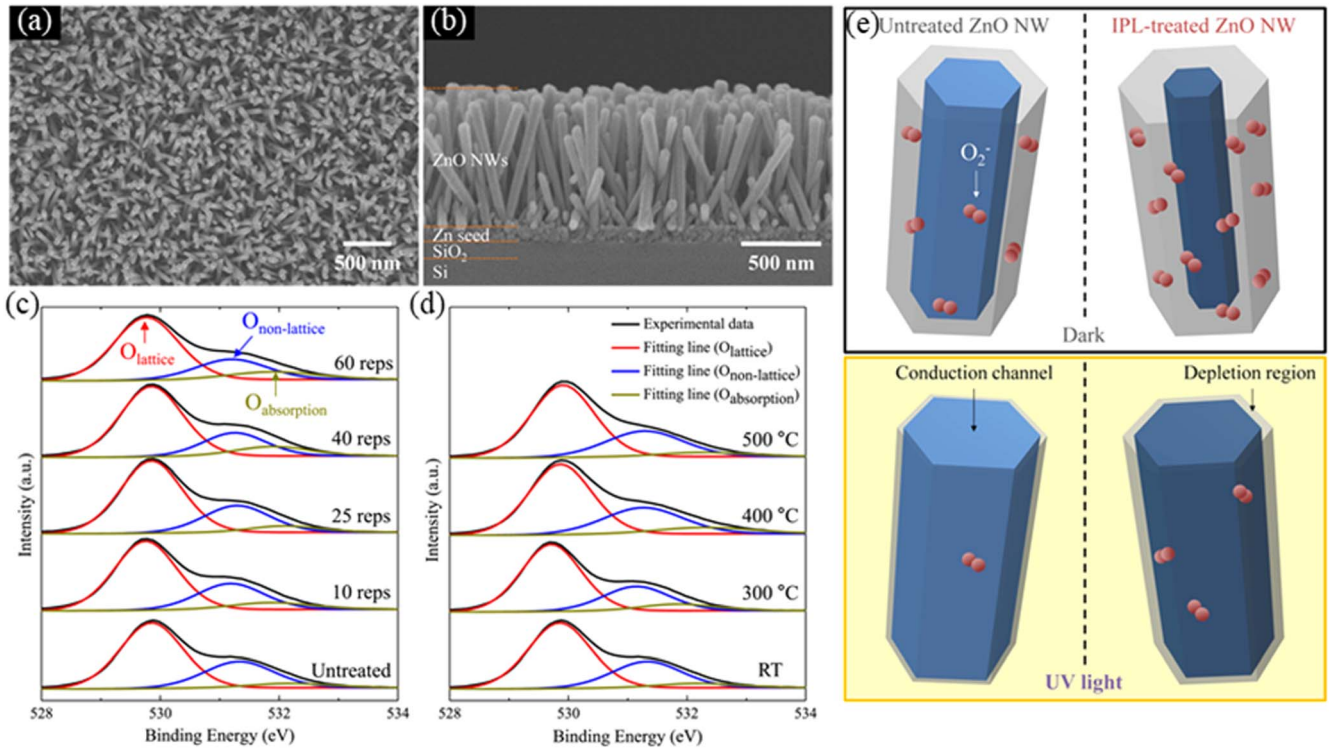

Figure 16. IPL annealing of ZnO nanowires for photodetector application: (a), (b) SEM images of ZnO nanowires, XPS spectra of the untreated, IPL annealed, and thermally annealed ZnO nanowires, O 1s spectrum of (c) IPL annealed ZnO nanowires and (d) thermally annealed ZnO nanowire, (e) schematic illustration of UV sensing mechanism. Reprinted from [123], copyright (2021), with permission from Elsevier.

condition is shown in figure 15(h). IPL-treated Co_3O_4 nanoparticles/CFP and Co nanoflakes/CFP samples were utilized as energy storage systems with reference to CFP only. It was proven that IPL-treated electrodes are able to fabricate energy storage devices with excellent current density.

The effects of IPL in terms of surface and interior using ZnO nanowires was analyzed [123]. They fabricated ultraviolet photodetectors (UV PDs) by IPL annealing of vertically aligned ZnO nanowires on SiO_2 (figures 16(a)–(b)) and analyzed the effect of IPL annealing through XPS. Compared with the thermal annealing, the XPS spectrum showed a different trend in the peaks of O 1s. The oxygen deficiency concentration on the surface and the binding force of Zn–O–Zn in the lattice increased (figures 16(c)–(d)). The increase in oxygen deficiency concentration on the surface is partly due to photoreduction by IPL light energy applied directly to the surface. The increase in the bonding force in the lattice is due to the heat generated by the absorption of the IPL light energy. IPL treatment is an effective process that can achieve both optical and thermal effects at the same time. The IPL annealed ZnO nanowires were applied as UV PDs, and the mechanism is shown in figure 16(e). UV PDs operate by modulating the surface state and depletion region. The IPL annealed ZnO nanowire increases the conductivity due to the increase in the bonding force of Zn–O–Zn in the lattice, and the depletion region is widened by the reduced surface, which increases the reactivity by UV. UV PDs with superior performance can be fabricated through IPL annealing.

The titanium dioxide (TiO_2) and SnO_2 nanoparticles were loaded onto multi-walled carbon nanotubes (MWCNTs) using IPL to implement a volatile organic compound sensor [124, 125]. MWCNTs were functionalized with nitric acid (HNO_3) to facilitate the loading of nanoparticles. On the surface of MWCNTs, COOH, C–OH and C=O groups were formed. However, this becomes a surface defect that impairs the electrical and mechanical properties of MWCNTs. IPL irradiation played a dual role in metal oxide nanoparticle grafted onto MWCNTs: (1) to revert the defective sites of carbon and (2) conversion of TiO_2 from anatase to rutile. Since anatase TiO_2 is unstable, it is gradually converted to rutile TiO_2 in ambient environment. It is also related to the performance of the sensor, so transformation to rutile TiO_2 is required [126–128]. In general, phase transformation of TiO_2 is performed by heat treatment at high temperature, but an effective phase change can be implemented using IPL.

3.3. Redox reaction from copper oxide to copper

Metal-based nanoparticles such as Au and Ag have been studied extensively for printed conductors due to their high conductivity, oxidation resistance and low melting point [129–131]. However, the high cost of noble metal nanoparticle-based nanoinks limits the commercialization as well as wide application [132]. For this reason, copper (Cu) nanoparticles are attracting attention as an alternative due to their low cost [133–135]. However, most Cu particles are suffering from oxidization in ambient conditions leading to

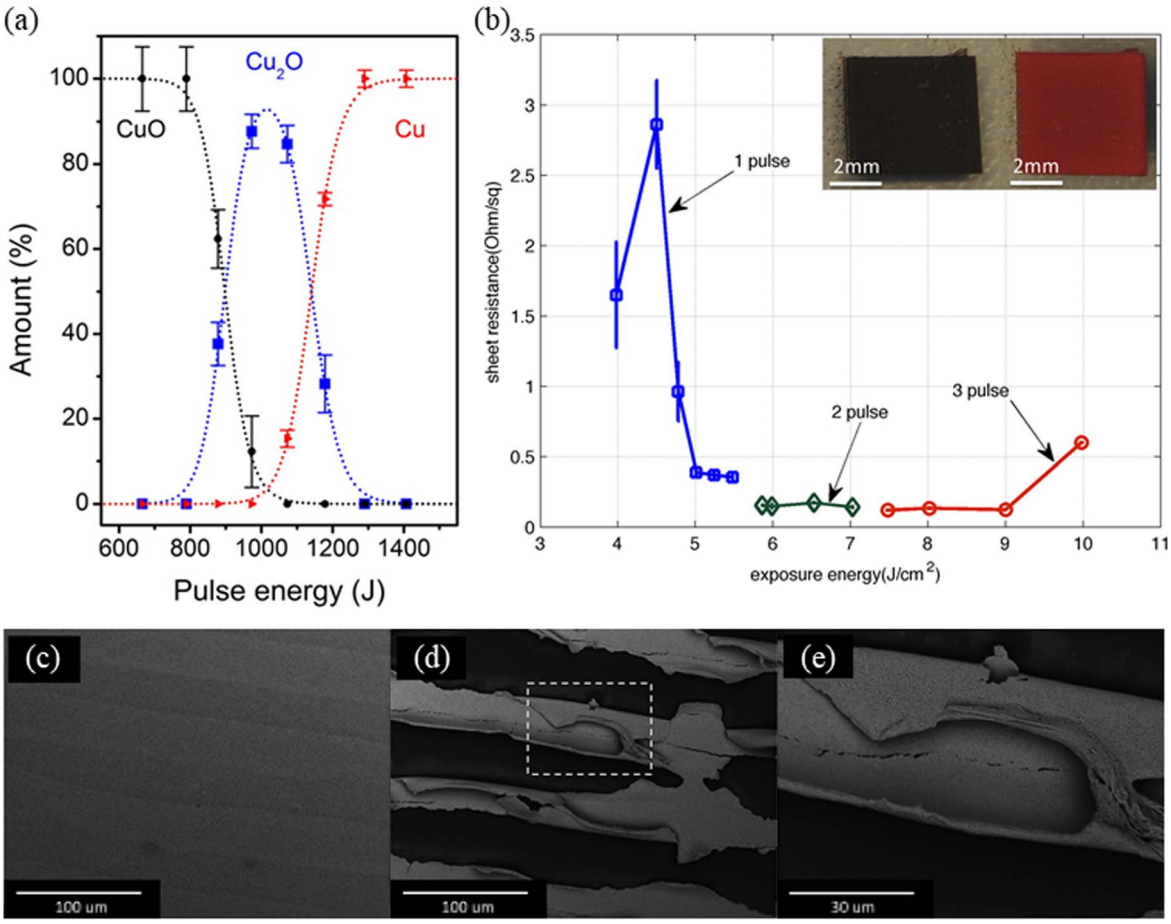

Figure 17. IPL reduction of CuO: (a) evolution of reduction of copper oxide to copper evaluated from the XRD diffraction data. Reprinted with permission from [137]. Copyright (2015) American Chemical Society. (b) Sheet resistance of sintered Cu layer, (c) SEM images of IPL sintered Cu layers (d) delaminated Cu layer in which the delamination follows the printing paths, (e) magnification of SEM images of the marked area of b to show the roll-up of the printed layer after IPL sintering with high energy. Reprinted with permission from [138]. Copyright 2014 American Chemical Society.

which oxide shell in nanostructure that hampers the sintering of Cu particles for electric conductors [136]. A reduction process using IPL was developed and widely used to obtain a high-conductivity Cu thin film without oxidation of Cu nanoparticles.

Francesco Paglia *et al* demonstrated that chemical reactions can be modulated and controlled simply by adjusting the IPL irradiation energy [137]. They investigated the reduction of CuO to metallic Cu via IPL sintering (figure 17(a)). By analyzing the growth of the crystalline phase, it was observed that the conversion of CuO to Cu_2O was observed with increasing IPL irradiation energy up to 1000 J/pulse. At the energy of ~1300 J/pulse, full conversion to metallic Cu can be possible. The IPL process allows the fabrication of highly conductive Cu electrodes with excellent mechanical properties and environmental stability by finely controlling the reduction parameters. Similarly, the effect of CuO printed on polyethylene terephthalate (PET) on IPL was reported [138]. The CuO layer was reduced to Cu with 30% conductivity of bulk Cu within 6 ms. Figure 17(b) shows the sheet resistance of Cu electrode according to the IPL sintering conditions. The sheet resistance of Cu is inversely proportional to the IPL irradiation energy. If the irradiation energy is less than 3.98 J cm^{-2}, sintering of the CuO layer is impossible. When the irradiation energy is 5.48 J cm^{-2}, the sheet resistance is optimized to 0.355 ohm sq^{-1}. The surface of the optimized Cu electrode is shown in figure 17(c). Energy above 5.86 J cm^{-2} causes partial delamination and damage to the electrode (figures 17(d)–(e)).

The reduction and sintering of CuO using IPL proved to be an effective process. Furthermore, Cu nanoparticles with CuO shells were systematically investigated to enhance the sintering effect, such as CuO shell thickness or the size of nanoparticles. The effect of CuO shell thickness on IPL sintering process was investigated as shown in figure 18(a) [139]. They fabricated Cu nanoparticles with various CuO shell thicknesses and measured the sheet resistance *in situ* during the IPL irradiation process (figure 18(b)). When the thickness of the shell is less than 3.6 nm, the sheet resistance is effectively reduced. On the other hand, there was a slight decrease at 7.1 nm and no change at 12.6 nm. The thick CuO shell was not suitable for the IPL sintering process due to its low reduction rate. They suggested the maximum allowable thickness of the CuO shell that allowed IPL sintering and provided the optimal amount of poly(N-vinylpyrrolidone) (PVP) in Cu nanoparticles for a specific CuO shell. It was also

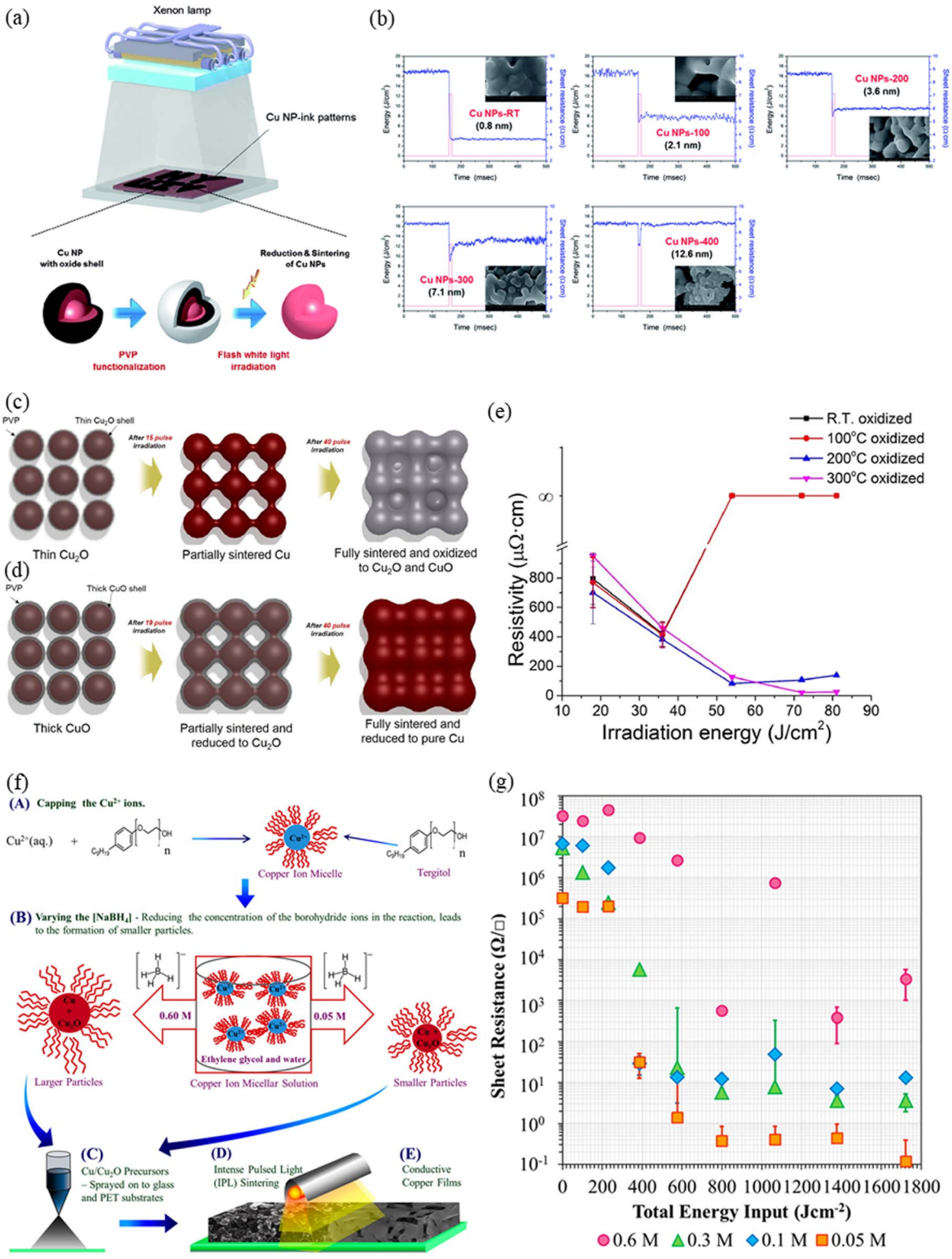

Figure 18. IPL reduction of Cu–CuO nanoparticles: (a) schematics controlling Cu oxide shell thickness, (b) *in situ* measurement of sheet resistance of Cu films with copper oxide shell formed at various temperatures during IPL treatment (irradiation energy: 12.5 J cm^{-2}, pulse time: 10 ms, 1 pulse). Reprinted with permission from [139]. Copyright 2017 Royal Society of Chemistry. (c), (d) Schematics of IPL sintering with multiple pulses in thin Cu_2O and thick CuO, (e) comparison of resistivity sintered with multiple pulses. Reprinted from [141], copyright (2021), with permission from Elsevier. (f) schematic fabrication process for conductive copper film by IPL reduction of Cu–CuO nanoparticles, (g) sheet resistance versus total energy input during the IPL sintering. Reprinted with permission from [142]. Copyright 2013 American Chemical Society.

demonstrated in detail that PVP functionalization effectively enhances the reduction of the shell by Jongeun Ryu *et al* [140]. IPL irradiation energy can overheat the surface of Cu nanoparticles to instantly generate energetic copper ions. At the same time, IPL converts the PVP chains to primary alcohols, secondary alcohols, carboxylic acids or acetic acids via photolysis events associated with OH radical attack. Alcohol and acid reduction mechanisms have been known for decades as the common pathways for metal oxide reduction. Therefore, the intermediate alcohols and acids can reduce the copper oxide shell of the superheated copper nanoparticles, and the PVP is degraded by the superheated copper nanoparticles and all removed. The effect of CuO shell type and thickness for fully sintering with multiple pulse IPL was investigated [141]. Irradiating the energy higher than enough may cause reoxidation of the Cu (figure 18(c)). To address this issue, they attempted to completely sinter the Cu without reoxidation by increasing the thickness of the CuO shell. The CuO shell was intentionally formed in a heating chamber at 100 °C to 300 °C. The CuO shell formed at 300 °C was completely reduced without reoxidation at a high IPL irradiation energy of 72 J cm^{-2} because it requires a lot of energy for reduction to Cu. As a result, the Cu thin film was completely sintered (figures 18(d), (e)). Similarly, the size and Cu/Cu_2O ratio of nanoparticles were controlled by changing the concentration of sodium borohydride ($NaBH_4$) during the synthesis of Cu/Cu_2O nanoparticles, and the relationship with the IPL energy required for fully sintering was investigated (figure 18(f)) [142]. As the concentration of $NaBH_4$ increased, the size of nanoparticles increased: nanoparticles of 10–15 nm and 100–120 nm from 0.05 to 0.6 M $NaBH_4$, respectively. The higher the concentration of $NaBH_4$, the higher the proportion of Cu nanoparticles produced: $Cu:Cu_2O = 34.12\%:65.88\%$ in 0.05 M, 91.56%:8.44% in 0.6 M, respectively. Figure 18(g) shows the change in sheet resistance according to $NaBH_4$ concentration and IPL irradiation energy. Cu/Cu_2O nanoparticles with a high Cu_2O ratio are completely sintered at high IPL irradiation energy, resulting in lower sheet resistance. On the other hand, in nanoparticles having a high Cu ratio, the sheet resistance is lowered at low IPL irradiation energy, and the sheet resistance is increased again at high IPL irradiation energy. This is due to the reoxidation taking place after complete sintering.

4. Conclusion

In this review, we summarize and review previous studies on IPL annealing and sintering based on metal oxide thin films and nanostructures. Unlike the metal, metal oxide material requires more energy in the sintering or annealing post-treatment process. Moreover, it has low absorbance for IPL since it is transparent at the wavelength wider than metal. For this reason, it requires higher energy in the IPL post-treatment process. Various techniques have been studied for addressing these issues. The IPL process has been improved by introducing auxiliary energy sources such as thermal heating and UV irradiation, which could be applied precedingly or concurrently with IPL process. Lower energy of IPL itself was also used in order to facilitate the post-treatment process prior to IPL treatment with higher energy. Furthermore, the absorption was greatly enhanced by employing light absorption layer and back-reflector. The effect of IPL process on structure and/or property change was highly dependent on the properties of the target material and substrates as well as conditions of IPL such as irradiation energy, pulse/off time, and number of pulses. This review shows that the photothermal and photoredox effect of IPL can improve the performance of metal oxides in a very short process time. It is certain that the IPL process will become a revolutionary post-treatment process for many applications with a variety of techniques in the near future.

Acknowledgments

This paper was supported by Konkuk University in 2018.

Data availability statement

No new data were created or analysed in this study.

ORCID iDs

Dongjin Lee https://orcid.org/0000-0002-7575-868X

References

[1] Samotaev N, Vasilyev V, Malkin E, Gromov E, Belyakov V, Golovin A, Pershenkov V, Ivanov I, Shaltaeva Y and Matusko M 2015 System for Synchronous Detection Trace of Explosives and Drags Substances on Human Fingers *Procedia Engineering* **120** 1050–3

[2] Fuse K, Tanimura H, Aoyama T, Kato S and Kobayashi I 2017 Conformal SDE doping for FinFETs using an arsenic-doped Sol-Gel Coating (SGC) and Flash Lamp Annealing (FLA) *2017 17th International Workshop on Junction Technology (IWJT) (Uji, Japan, 1–2 June 2017)* (IEEE) pp 66–8

[3] Muydinov R, Seeger S, Vinoth Kumar S H B, Klimm C, Kraehnert R, Wagner M R and Szyszka B 2018 Crystallisation behaviour of $CH_3NH_3PbI_3$ films: the benefits of sub-second flash lamp annealing *Thin Solid Films* **653** 204–14

[4] Wirth H, Panknin D, Skorupa W and Niemann E 1999 Efficient p-type doping of 6H-SiC: flash-lamp annealing after aluminum implantation *Appl. Phys. Lett.* **74** 979–81

[5] Bakhteeva N D, Todorova E V, Kannykin S V, Vasiliev A L and Kolobylina N N 2018 Flash lamp annealing of amorphous Al–Fe–Ni–La alloys *J. Phys. Conf.* **1134** 012005

[6] Gebel T, Voelskow M, Skorupa W, Mannino G, Privitera V, Priolo F, Napolitani E and Carnera A 2002 Flash lamp annealing with millisecond pulses for ultra-shallow boron profiles in silicon *Nucl. Instrum. Methods Phys. Res.* B **186** 287–91

[7] Bregolin F L, Krockert K, Prucnal S, Vines L, Hübner R, Svensson B G, Wiesenhütter K, Möller H J and Skorupa W 2014 Hydrogen engineering via plasma immersion ion implantation and flash lamp annealing in silicon-based solar cell substrates *J. Appl. Phys.* **115** 064505

[8] Smith M, McMahon R A, Voelskow M and Skorupa W 2004 Modeling and regrowth mechanisms of flash lamp processing of SiC-on-silicon heterostructures *J. Appl. Phys.* **96** 4843–51

[9] Kim H-S, Dhage S R, Shim D-E and Hahn H T 2009 Intense pulsed light sintering of copper nanoink for printed electronics *Appl. Phys.* A **97** 791

[10] Ghahremani A H, Pishgar S, Bahadur J and Druffel T 2020 Intense pulse light annealing of perovskite photovoltaics using gradient flashes *ACS Appl. Energy Mater.* **3** 11641–54

[11] Meng L, Zhang Y, Yang X and Zhang J 2019 Atomistic modeling of resistivity evolution of copper nanoparticle in intense pulsed light sintering process *Physica* B **554** 31–4

[12] Niittynen J, Sowade E, Kang H, Baumann R R and Mäntysalo M 2015 Comparison of laser and intense pulsed light sintering (IPL) for inkjet-printed copper nanoparticle layers *Sci. Rep.* **5** 8832

[13] Draper G L, Dharmadasa R, Staats M E, Lavery B W and Druffel T 2015 Fabrication of elemental copper by intense pulsed light processing of a copper nitrate hydroxide ink *ACS Appl. Mater. Interfaces* **7** 16478–85

[14] Albrecht A, Rivadeneyra A, Abdellah A, Lugli P and Salmerón J F 2016 Inkjet printing and photonic sintering of silver and copper oxide nanoparticles for ultra-low-cost conductive patterns *J. Mater. Chem.* C **4** 3546–54

[15] Mitra D, Mitra K Y, Hartwig M and Baumann R R 2016 Intense pulsed light sintering of an inkjet printed silver nanoparticle ink depending on the spectral absorption and reflection of the background *NIP Digit. Fabr. Conf.* **2016** 309–13

[16] Weise D, Mitra K Y, Sowade E and Baumann R R 2015 Intense pulsed light sintering of inkjet printed silver nanoparticle ink: influence of flashing parameters and substrate *MRS Online Proc. Libr.* **1761** 504

[17] Sowade E, Kang H, Mitra K Y, Weiß O J, Weber J and Baumann R R 2015 Roll-to-roll infrared (IR) drying and sintering of an inkjet-printed silver nanoparticle ink within 1 s *J. Mater. Chem.* C **3** 11815–26

[18] Kang J S, Ryu J, Kim H S and Hahn H T 2011 Sintering of inkjet-printed silver nanoparticles at room temperature using intense pulsed light *J. Electron. Mater.* **40** 2268

[19] Yoo T-H, Kwon S-J, Kim H-S, Hong J-M, Lim J A and Song Y-W 2014 Sub-second photo-annealing of solution-processed metal oxide thin-film transistors via irradiation of intensely pulsed white light *RSC Adv.* **4** 19375–9

[20] Jo J-W, Kim K-T, Park H-H, Park S K, Heo J S, Kim I and Lee M-J 2019 High-speed and low-temperature atmospheric photo-annealing of large-area solution-processed IGZO thin-film transistors by using programmable pulsed operation of xenon flash lamp *J. Korean Phys. Soc.* **74** 1052–8

[21] Kim H J, Han C J, Yoo B, Lee J, Lee K, Lee K H and Oh M S 2020 Effects of intense pulsed light (IPL) rapid annealing and back-channel passivation on solution-processed In–Ga–Zn–O thin film transistors array *Micromachines* **11** 508

[22] Tetzner K, Lin Y-H, Regoutz A, Seitkhan A, Payne D J and Anthopoulos T D 2017 Sub-second photonic processing of solution-deposited single layer and heterojunction metal oxide thin-film transistors using a high-power xenon flash lamp *J. Mater. Chem.* C **5** 11724–32

[23] Jeong H-J, Lee H-M, Ryu C-H, Park E-J, Han K-L, Hwang H-J, Ok K-C, Kim H-S and Park J-S 2019 Ultra-high-speed intense pulsed-light irradiation technique for high-performance zinc oxynitride thin-film transistors *ACS Appl. Mater. Interfaces* **11** 4152–8

[24] Kim Y, Kim J, Kim B, Kim H J, Kim S, Choi E, Hwang J-H and Park S 2017 Application of flash lamp annealing on nitrogen-doped amorphous indium–gallium–zinc–oxide thin film transistors *ECS J. Solid State Sci. Technol.* **6** P778–85

[25] O'Connor É, Halter M, Eltes F, Sousa M, Kellock A, Abel S and Fompeyrine J 2018 Stabilization of ferroelectric Hf_xZr_1–xO_2 films using a millisecond flash lamp annealing technique *APL Mater.* **6** 121103

[26] Henke T, Knaut M, Hossbach C, Geidel M, Albert M and Bartha J W 2017 Growth of aluminum oxide thin films with enhanced film density by the integration of *in situ* flash annealing into low-temperature atomic layer deposition *Surf. Coat. Technol.* **309** 600–8

[27] Lehmann J, Hübner R, Borany J V, Skorupa W, Mikolajick T, Schäfer A, Schubert J and Mantl S 2013 Millisecond flash lamp annealing for $LaLuO_3$ and $LaScO_3$ high-k dielectrics *Microelectron. Eng.* **109** 381–4

[28] Lehmann J, Shevchenko N, Mücklich A, Borany J V, Skorupa W, Schubert J, Lopez J M J and Mantl S 2011 Millisecond flash-lamp annealing of $LaLuO_3$ *Microelectron. Eng.* **88** 1346–8

[29] Kim K, Woo J Y, Jeong S and Han C-S 2011 Photoenhancement of a quantum dot nanocomposite via UV annealing and its application to white LEDs *Adv. Mater.* **23** 911–4

[30] Lu L, Echizen M, Nishida T, Ishikawa Y, Uchiyama K and Uraoka Y 2012 Low-temperature fabrication of solution-processed InZnO thin-film transistors with Si impurities by UV/O_3-assisted annealing *AIP Adv.* **2** 032111

[31] Hwang Y H, Seo S-J, Jeon J-H and Bae B-S 2012 Ultraviolet photo-annealing process for low temperature processed sol-gel zinc tin oxide thin film transistors *Electrochem. Solid-State Lett.* **15** H91

[32] Bruno E, Scapellato G G, Bisognin G, Carria E, Romano L, Carnera A and Priolo F 2010 High-level incorporation of antimony in germanium by laser annealing *J. Appl. Phys.* **108** 124902

[33] You P, Li G, Tang G, Cao J and Yan F 2020 Ultrafast laser-annealing of perovskite films for efficient perovskite solar cells *Energy Environ. Sci.* **13** 1187–96

[34] Chen M-F, Lin K-M and Ho Y-S 2012 Laser annealing process of ITO thin films using beam shaping technology *Opt. Lasers Eng.* **50** 491–5

[35] Jang Y-R, Joo S-J, Chu J-H, Uhm H-J, Park J-W, Ryu C-H, Yu M-H and Kim H-S 2021 A review on intense pulsed light sintering technologies for conductive electrodes in printed electronics *Int. J. Precis. Eng. Manuf.-Green Technol.* **8** 327–63

[36] Park J, Nam D, Park S and Lee D 2018 Fabrication of flexible strain sensors via roll-to-roll gravure printing of silver ink *Smart Mater. Struct.* **27** 085014

[37] Huang Q and Zhu Y 2018 Gravure printing of water-based silver nanowire ink on plastic substrate for flexible electronics *Sci. Rep.* **8** 15167

[38] Park J, Nguyen H A D, Park S, Lee J, Kim B and Lee D 2015 Roll-to-roll gravure printed silver patterns to guarantee printability and functionality for mass production *Curr. Appl Phys.* **15** 367–76

[39] Shin K-H, Nguyen H A D, Park J, Shin D and Lee D 2017 Roll-to-roll gravure printing of thick-film silver electrode micropatterns for flexible printed circuit board *J. Coat. Technol. Res.* **14** 95–106

[40] Pan H, Ko S H and Grigoropoulos C P 2008 Thermal sintering of solution-deposited nanoparticle silver ink films characterized by spectroscopic ellipsometry *Appl. Phys. Lett.* **93** 234104

[41] Denneulin A, Blayo A, Neuman C and Bras J 2011 Infra-red assisted sintering of inkjet printed silver tracks on paper substrates *J. Nanopart. Res.* **13** 3815–23

[42] Cherrington M, Claypole T C, Deganello D, Mabbett I, Watson T and Worsley D 2011 Ultrafast near-infrared sintering of a slot-die coated nano-silver conducting ink *J. Mater. Chem.* **21** 7562–4
[43] Qin G and Watanabe A 2014 Conductive network structure formed by laser sintering of silver nanoparticles *J. Nanopart. Res.* **16** 2684
[44] Peng P, Hu A and Zhou Y 2012 Laser sintering of silver nanoparticle thin films: microstructure and optical properties *Appl. Phys.* A **108** 685–91
[45] Allen M, Alastalo A, Suhonen M, Mattila T, Leppäniemi J and Seppa H 2011 Contactless electrical sintering of silver nanoparticles on flexible substrates *IEEE Trans. Microwave Theory Tech.* **59** 1419–29
[46] Allen M L, Aronniemi M, Mattila T, Alastalo A, Ojanperä K, Suhonen M and Seppä H 2008 Electrical sintering of nanoparticle structures *Nanotechnology* **19** 175201
[47] Wünscher S, Stumpf S, Teichler A, Pabst O, Perelaer J, Beckert E and Schubert U S 2012 Localized atmospheric plasma sintering of inkjet printed silver nanoparticles *J. Mater. Chem.* **22** 24569–76
[48] Ma S, Bromberg V, Liu L, Egitto F D, Chiarot P R and Singler T J 2014 Low temperature plasma sintering of silver nanoparticles *Appl. Surf. Sci.* **293** 207–15
[49] Perelaer J, de Gans B J and Schubert U S 2006 Ink-jet printing and microwave sintering of conductive silver tracks *Adv. Mater.* **18** 2101–4
[50] Kim K-S, Park B-G, Jung K-H, Kim J-W, Jeong M Y and Jung S-B 2015 Microwave sintering of silver nanoink for radio frequency applications *J. Nanosci. Nanotechnol.* **15** 2333–7
[51] Ding S, Jiu J, Tian Y, Sugahara T, Nagao S and Suganuma K 2015 Fast fabrication of copper nanowire transparent electrodes by a high intensity pulsed light sintering technique in air *PCCP* **17** 31110–6
[52] Song C-H, Ok K-H, Lee C-J, Kim Y, Kwak M-G, Han C J, Kim N, Ju B-K and Kim J-W 2015 Intense-pulsed-light irradiation of Ag nanowire-based transparent electrodes for use in flexible organic light emitting diodes *Org. Electron.* **17** 208–15
[53] Dexter M, Pfau A, Gao Z, Herman G S, Chang C-H and Malhotra R 2018 Modeling nanoscale temperature gradients and conductivity evolution in pulsed light sintering of silver nanowire networks *Nanotechnology* **29** 505205
[54] Zhong Z, Woo K, Kim I, Hwang H, Kwon S, Choi Y-M, Lee Y, Lee T-M, Kim K and Moon J 2016 Roll-to-roll-compatible, flexible, transparent electrodes based on self-nanoembedded Cu nanowires using intense pulsed light irradiation *Nanoscale* **8** 8995–9003
[55] Jiu J, Nogi M, Sugahara T, Tokuno T, Araki T, Komoda N, Suganuma K, Uchida H and Shinozaki K 2012 Strongly adhesive and flexible transparent silver nanowire conductive films fabricated with a high-intensity pulsed light technique *J. Mater. Chem.* **22** 23561–7
[56] Chung W-H, Jang Y-R, Hwang Y-T, Kim S-H and Kim H-S 2020 The surface plasmonic welding of silver nanowires via intense pulsed light irradiation combined with NIR for flexible transparent conductive films *Nanoscale* **12** 17725–37
[57] Klasens H A and Koelmans H 1964 A tin oxide field-effect transistor *Solid State Electron.* **7** 701–2
[58] Kulchaisit C, Bermundo J P S, Fujii M N, Ishikawa Y and Uraoka Y 2018 High performance top gate a-IGZO TFT utilizing siloxane hybrid material as a gate insulator *AIP Adv.* **8** 095001
[59] Ahn M H, Cho E S and Kwon S J 2014 Characteristics of ITO-resistive touch film deposited on a PET substrate by in-line DC magnetron sputtering *Vacuum* **101** 221–7
[60] Yang Y, Huang Q, Metz A W, Ni J, Jin S, Marks T J, Madsen M E, DiVenere A and Ho S T 2004 High-performance organic light-emitting diodes using ITO anodes grown on plastic by room- temperature ion-assisted deposition *Adv. Mater.* **16** 321–4
[61] Shikoh A S, Ahmad Z, Touati F, Shakoor R A and Al-Muhtaseb S A 2017 Optimization of ITO glass/TiO_2 based DSSC photo-anodes through electrophoretic deposition and sintering techniques *Ceram. Int.* **43** 10540–5
[62] Shen W, Zhao Y and Zhang C 2005 The preparation of ZnO based gas-sensing thin films by ink-jet printing method *Thin Solid Films* **483** 382–7
[63] Choi E K, Park J, Kim B S and Lee D 2015 Fabrication of electrodes and near-field communication tags based on screen printing of silver seed patterns and copper electroless plating *Int. J. Precis. Eng. Manuf.* **16** 2199–204
[64] Jeong H, Park S, Lee J, Won P, Ko S H and Lee D 2018 Fabrication of transparent conductive film with flexible silver nanowires using roll-to-roll slot-die coating and calendering and its application to resistive touch panel *Adv. Electron. Mater.* **4** 1800243
[65] Sachse C, Weiß N, Gaponik N, Müller-Meskamp L, Eychmüller A and Leo K 2014 ITO-free, small-molecule organic solar cells on spray-coated copper-nanowire-based transparent electrodes *Adv. Energy Mater.* **4** 1300737
[66] Kumar M, Jeong H and Lee D 2018 Solution-processed high-mobility ZnO thin film transistors based on multiple-stacked channel layer doped with Hf and Mg *Superlattices Microstruct.* **120** 395–401
[67] Kathirgamanathan P, Kumaraverl M, Vanga R R and Ravichandran S 2018 Intense pulsed light (IPL) annealed sol-gel derived ZnO electron injector for the production of high efficiency inverted quantum dot light emitting devices (QLEDs) *RSC Adv.* **8** 36632–46
[68] Zhu M, Liu W, Ke W, Clark S, Secor E B, Song T-B, Kanatzidis M G, Li X and Hersam M C 2017 Millisecond-pulsed photonically-annealed tin oxide electron transport layers for efficient perovskite solar cells *J. Mater. Chem.* A **5** 24110–5
[69] Eom T-Y, Ahn C-H, Kang J-G, Salman M S, Lee S-Y, Kim Y-H, Lee H-J, Kang C-M and Kang C 2018 Investigation of the evolution of nitrogen defects in flash-lamp-annealed InGaZnO films and their effects on transistor characteristics *Appl. Phys. Express* **11** 061104
[70] Park K, Woo K, Kim J, Lee D, Ahn Y, Song D, Kim H, Oh D, Kwon S and Lee Y 2019 High-resolution and large-area patterning of highly conductive silver nanowire electrodes by reverse offset printing and intense pulsed light irradiation *ACS Appl. Mater. Interfaces* **11** 14882–91
[71] Gokhale P, Mitra D, Sowade E, Mitra K Y, Gomes H L, Ramon E, Al-Hamry A, Kanoun O and Baumann R R 2017 Controlling the crack formation in inkjet-printed silver nanoparticle thin-films for high resolution patterning using intense pulsed light treatment *Nanotechnology* **28** 495301
[72] Kang J S, Ryu J, Kim H S and Hahn H T 2011 Sintering of inkjet-printed silver nanoparticles at room temperature using intense pulsed light *J. Electron. Mater.* **40** 2268–77
[73] Kang C, Kim H, Oh Y, Baek K and Do L 2016 High-performance, solution-processed indium-oxide TFTs using rapid flash lamp annealing *IEEE Electron Device Lett.* **37** 595–8
[74] Moon C-J and Kim H-S 2019 Intense pulsed light annealing process of indium–gallium–zinc–oxide semiconductors via flash white light combined with deep-UV and near-infrared drying for high-performance thin-film transistors *ACS Appl. Mater. Interfaces* **11** 13380–8
[75] Song P K, Shigesato Y, Kamei M and Yasui I 1999 Electrical and structural properties of tin-doped indium oxide films deposited by DC sputtering at room temperature *Jpn. J. Appl. Phys.* **38** 2921
[76] Venkataraj S, Kappertz O, Weis H, Drese R, Jayavel R and Wuttig M 2002 Structural and optical properties of thin

zirconium oxide films prepared by reactive direct current magnetron sputtering *J. Appl. Phys.* **92** 3599–607
[77] Noh J H, Ryu S Y, Jo S J, Kim C S, Sohn S, Rack P D, Kim D and Baik H K 2010 Indium oxide thin-film transistors fabricated by RF sputtering at room temperature *IEEE Electron Device Lett.* **31** 567–9
[78] Belo G S, da Silva B J P, de Vasconcelos E A, de Azevedo W M and da Silva E F 2008 A simplified reactive thermal evaporation method for indium tin oxide electrodes *Appl. Surf. Sci.* **255** 755–7
[79] Al-Kuhaili M F, Durrani S M A and Khawaja E E 2003 Optical properties of gallium oxide films deposited by electron-beam evaporation *Appl. Phys. Lett.* **83** 4533
[80] Rossall A K, van den Berg J A, Meehan D, Rajendiran S and Wagenaars E 2019 Analysis of plasma enhanced pulsed laser deposition of transition metal oxide thin films using medium energy ion scattering *Nucl. Instrum. Methods Phys. Res.* B **450** 274–8
[81] Groner M D, Fabreguette F H, Elam J W and George S M 2004 Low-temperature Al_2O_3 atomic layer deposition *Chem. Mater.* **16** 639–45
[82] Lee Y-C *et al* 2009 Rapid thermal annealing effects on the structural and optical properties of ZnO films deposited on Si substrates *J. Lumin.* **129** 148–52
[83] Hsieh J H, Kuo P W, Peng K C, Liu S J, Hsueh J D and Chang S C 2008 Opto-electronic properties of sputter-deposited Cu_2O films treated with rapid thermal annealing *Thin Solid Films* **516** 5449–53
[84] Kim Y, Park S, Kim S, Kim B-K, Choi Y, Hwang J-H and Kim H J 2017 Flash lamp annealing of indium tin oxide thin-films deposited on polyimide backplanes *Thin Solid Films* **628** 88–95
[85] Kim Y, Park S, Kim B-K, Kim H J and Hwang J-H 2015 Xe-arc flash annealing of indium tin oxide thin-films prepared on glass backplanes *Int. J. Heat Mass Transfer* **91** 543–51
[86] Jeon S R, Han S W and Park J W 1995 Effect of rapid thermal annealing treatment on electrical properties and microstructure of tantalum oxide thin film deposited by plasma-enhanced chemical vapor deposition *J. Appl. Phys.* **77** 5978–81
[87] Xue X-T, Gu Y, Ma H-P, Hang C-Z, Tao J-J, Lu H-L and Zhang D W 2020 Effect of rapid thermal annealing on the properties of zinc tin oxide films prepared by plasma-enhanced atomic layer deposition *Ceram. Int.* **46** 13033–9
[88] Song S, Yang T, Liu J, Xin Y, Li Y and Han S 2011 Rapid thermal annealing of ITO films *Appl. Surf. Sci.* **257** 7061–4
[89] Djurišić A B, Leung Y H and Ching Ng A M 2014 Strategies for improving the efficiency of semiconductor metal oxide photocatalysis *Mater. Horiz.* **1** 400–10
[90] Thomas S R, Pattanasattayavong P and Anthopoulos T D 2013 Solution-processable metal oxide semiconductors for thin-film transistor applications *Chem. Soc. Rev.* **42** 6910–23
[91] Wang C, Yin L, Zhang L, Xiang D and Gao R 2010 Metal oxide gas sensors: sensitivity and influencing factors *Sensors* **10** 2088–106
[92] Zhang M, de Respinis M and Frei H 2014 Time-resolved observations of water oxidation intermediates on a cobalt oxide nanoparticle catalyst *Nat. Chem.* **6** 362–7
[93] Zhang D, Chang H, Li P, Liu R and Xue Q 2016 Fabrication and characterization of an ultrasensitive humidity sensor based on metal oxide/graphene hybrid nanocomposite *Sensors Actuators* B **225** 233–40
[94] Hong S, Kim Y and Han J 2008 Development of ultrafine indium tin oxide (ITO) nanoparticle for ink-jet printing by low-temperature synthetic method *IEEE Trans. Nanotechnol.* **7** 172–6
[95] Shao D, Yu M, Sun H, Hu T, lian J and Sawyer S 2013 High responsivity, fast ultraviolet photodetector fabricated from ZnO nanoparticle–graphene core–shell structures *Nanoscale* **5** 3664–7
[96] Ren H, Hassna O, Li J and Arigong B 2021 A patterned phase-changing vanadium dioxide film stacking with VO_2 nanoparticle matrix for high performance energy-efficient smart window applications *Appl. Phys. Lett.* **118** 051901
[97] Chen J-Z, Ko W-Y, Yen Y-C, Chen P-H and Lin K-J 2012 Hydrothermally processed TiO_2 nanowire electrodes with antireflective and electrochromic properties *ACS Nano* **6** 6633–9
[98] Tao Y, Fu M, Zhao A, He D and Wang Y 2010 The effect of seed layer on morphology of ZnO nanorod arrays grown by hydrothermal method *J. Alloys Compd.* **489** 99–102
[99] Zhang Y, Chen C, Wu W, Niu F, Liu X, Zhong Y, Cao Y, Liu X and Huang C 2013 Facile hydrothermal synthesis of vanadium oxides nanobelts by ethanol reduction of peroxovanadium complexes *Ceram. Int.* **39** 129–41
[100] Yuan C, Zhang L, Hou L, Pang G and Oh W-C 2014 One-step hydrothermal fabrication of strongly coupled Co_3O_4 nanosheets–reduced graphene oxide for electrochemical capacitors *RSC Adv.* **4** 14408–13
[101] Shi R, Yang P, Dong X, Ma Q and Zhang A 2013 Growth of flower-like ZnO on ZnO nanorod arrays created on zinc substrate through low-temperature hydrothermal synthesis *Appl. Surf. Sci.* **264** 162–70
[102] Shen G, Chen P-C, Ryu K and Zhou C 2009 Devices and chemical sensing applications of metal oxide nanowires *J. Mater. Chem.* **19** 828–39
[103] Kobayashi Y, Hata H, Salama M and Mallouk T E 2007 Scrolled sheet precursor route to niobium and tantalum oxide nanotubes *Nano Lett.* **7** 2142–5
[104] Sarabadani P, Sadeghi M, Ghasemi M, Asadollahi Z and Afshari N 2011 Synthesis and characterization of tin oxide nanoparticles by solid state chemical reaction method *J. Cluster Sci.* **22** 131–40
[105] Yang Q, Lu Z, Liu J, Lei X, Chang Z, Luo L and Sun X 2013 Metal oxide and hydroxide nanoarrays: Hydrothermal synthesis and applications as supercapacitors and nanocatalysts *Prog. Nat. Sci. Mater. Int.* **23** 351–66
[106] Soultanidis N, Zhou W, Kiely C J and Wong M S 2012 Solvothermal synthesis of ultrasmall tungsten oxide nanoparticles *Langmuir* **28** 17771–7
[107] Sui R and Charpentier P 2012 Synthesis of metal oxide nanostructures by direct sol-gel chemistry in supercritical fluids *Chem. Rev.* **112** 3057–82
[108] Yoo T-H, Kim S M, Lim J A, Kim J-H, Sang B-I and Song Y-W 2013 High-speed annealing of hydrous ruthenium oxide nanoparticles by intensely pulsed white light for supercapacitors *J. Electrochem. Soc.* **160** A1772–6
[109] Choi S-J, Jang J-S, Park H J and Kim I-D 2017 Optically sintered 2D RuO_2 nanosheets: temperature-controlled NO_2 reaction *Adv. Funct. Mater.* **27** 1606026
[110] Patil S A, Hwang H-J, Yu M-H, Shrestha N K and Kim H-S 2017 Photonic sintering of a ZnO nanosheet photoanode using flash white light combined with deep UV irradiation for dye-sensitized solar cells *RSC Adv.* **7** 6565–73
[111] Yamaguchi Y, Kanamaru Y, Fukushima M, Fujimoto K and Ito S 2015 Preparation of highly crystallized strontium titanate powders at room temperature *J. Am. Ceram. Soc.* **98** 3054–61
[112] Yamaguchi Y, Ando D, Ito S and Fujimoto K 2016 Novel room temperature synthesis process of $SrTiO_3$ fine particles and its photocatalytic property *J. Jpn. Soc. Powder Powder Metall.* **63** 559–62
[113] Lin Y S, Yang Q and Ida J 2009 High temperature sorption of carbon dioxide on perovskite-type metal oxides *J. Taiwan Inst. Chem. Eng.* **40** 276–80
[114] Park J, Lim Y, Kong S, Lee H and Kim Y-B 2019 Rapid fabrication of chemical solution-deposited lanthanum nickelate thin films via intense pulsed-light process *Coatings* **9** 372

[115] Park J-S, Lee H, Heo S and Kim Y B 2020 Heater-assisted intense pulsed light irradiation for lanthanum strontium cobaltite thin film electrode fabrication *Thin Solid Films* **697** 137778
[116] Han Y J, Kang K-T, Ju B-K and Cho K H 2020 Effect of time-dependent characteristics of ZnO nanoparticles electron transport layer improved by intense-pulsed light post-treatment on hole-electron injection balance of quantum-dot light-emitting diodes *Materials* **13** 5041
[117] Tang P, Wei C, Xie L, Chen X, Li X, Bai S, Su W, Wang F and Cui Z 2020 Efficiency enhancement of quantum-dot light-emitting diodes via rapid post-treatment of intense pulsed light sintering technique *Chem. Phys. Lett.* **739** 137048
[118] Kim K-S, Son E-W, Youn J W and Kim D U 2019 Intense-pulsed-light irradiation compared to thermal heating for fabrication of VO_2 nanoparticle-based thermochromic films *Appl. Surf. Sci.* **486** 219–27
[119] Kim K-S, Son E-W, Youn J W and Kim D U 2019 Intense pulsed light sintering of vanadium dioxide nanoparticle films and their optical properties for thermochromic smart window *Mater. Des.* **176** 107838
[120] Jang K, Yu S, Park S-H, Kim H-S and Ahn H 2015 Intense pulsed light-assisted facile and agile fabrication of cobalt oxide/nickel cobaltite nanoflakes on nickel-foam for high performance supercapacitor applications *J. Alloys Compd.* **618** 227–32
[121] Park C, Hwang J, Hwang Y-T, Song C, Ahn S, Kim H-S and Ahn H 2017 Intense pulsed white light assisted fabrication of Co-CoO_x core–shell nanoflakes on graphite felt for flexible hybrid supercapacitors *Electrochim. Acta* **246** 757–65
[122] Lee S, Park S-H, Jang K, Yu S, Song C, Kim H-S and Ahn H 2017 Simple, ultra-rapid, versatile method to synthesize cobalt/cobalt oxide nanostructures on carbon fiber paper via intense pulsed white light (IPWL) photothermal reduction for energy storage applications *J. Alloys Compd.* **724** 684–94
[123] Noh Y, Jeong H and Lee D 2021 Enhanced ultraviolet photodetector using zinc oxide nanowires with intense pulsed light post-treatment *J. Alloys Compd.* **871** 159537
[124] Wong D, Abuzalat O, Mostafa S, Kim S and Park S S 2019 Intense pulsed light conversion of anatase to rutile TiO_2 for hybrid TiO_2-SnO_2/MWCNTs/PVB room temperature VOCs sensor *IEEE Sens. J.* **19** 9113–21
[125] Wong D, Abuzalat O, Mostafa S, Park S S and Kim S 2020 Intense pulsed light-based synthesis of hybrid TiO_2–SnO_2/MWCNT doped Cu-BTC for room temperature ammonia sensing *J. Mater. Chem.* C **8** 7567–74
[126] Zhang J, Chen C, Lu H, Leng D, Li G, Liu Y, Liang Q, Gao J, Wang C and Zhu B 2020 Construction of anatase@rutile core@shell TiO_2 nanosheets with controllable shell layer thicknesses for enhanced ethanol sensing *Sensors Actuators* B **325** 128815
[127] Zhang Y, Fu W, Yang H, Qi Q, Zeng Y, Zhang T, Ge R and Zou G 2008 Synthesis and characterization of TiO_2 nanotubes for humidity sensing *Appl. Surf. Sci.* **254** 5545–7
[128] Hamdan S A, IbrahiM I M and Ali I M 2020 Comparison of anatase and rutile TiO_2 nanostructure for gas sensing application *Dig. J. Nanomater. Bios.* **15** 1001–8
[129] Gabrion X, Placet V, Trivaudey F and Boubakar L 2016 About the thermomechanical behaviour of a carbon fibre reinforced high-temperature thermoplastic composite *Composites* B **95** 386–94
[130] Woo K, Kim D, Kim J S, Lim S and Moon J 2009 Ink-jet printing of Cu–Ag-based highly conductive tracks on a transparent substrate *Langmuir* **25** 429–33
[131] Lee D J, Park S H, Jang S, Kim H S, Oh J H and Song Y W 2011 Pulsed light sintering characteristics of inkjet-printed nanosilver films on a polymer substrate *J. Micromech. Microeng.* **21** 125023
[132] Hwang H-J, Chung W-H and Kim H-S 2012 *In situ* monitoring of flash-light sintering of copper nanoparticle ink for printed electronics *Nanotechnology* **23** 485205
[133] Jang S, Seo Y, Choi J, Kim T, Cho J, Kim S and Kim D 2010 Sintering of inkjet printed copper nanoparticles for flexible electronics *Scripta Mater.* **62** 258–61
[134] Lee B, Kim Y, Yang S, Jeong I and Moon J 2009 A low-cure-temperature copper nano ink for highly conductive printed electrodes *Curr. Appl. Phys.* **9** e157–60
[135] Park B K, Jeong S, Kim D, Moon J, Lim S and Kim J S 2007 Synthesis and size control of monodisperse copper nanoparticles by polyol method *J. Colloid Interface Sci.* **311** 417–24
[136] Rager M S, Aytug T, Veith G M and Joshi P 2016 Low-thermal-budget photonic processing of highly conductive Cu interconnects based on CuO nanoinks: potential for flexible printed electronics *ACS Appl. Mater. Interfaces* **8** 2441–8
[137] Paglia F, Vak D, van Embden J, Chesman A S R, Martucci A, Jasieniak J J and Della Gaspera E 2015 Photonic sintering of copper through the controlled reduction of printed CuO nanocrystals *ACS Appl. Mater. Interfaces* **7** 25473–8
[138] Kang H, Sowade E and Baumann R R 2014 Direct intense pulsed light sintering of inkjet-printed copper oxide layers within six milliseconds *ACS Appl. Mater. Interfaces* **6** 1682–7
[139] Oh G-H, Hwang H-J and Kim H-S 2017 Effect of copper oxide shell thickness on flash light sintering of copper nanoparticle ink *RSC Adv.* **7** 17724–31
[140] Ryu J, Kim H-S and Hahn H T 2011 Reactive sintering of copper nanoparticles using intense pulsed light for printed electronics *J. Electron. Mater.* **40** 42–50
[141] Jang Y-R, Ryu C-H, Chu J-H, Nam J-B and Kim H-S 2021 Multiple intense pulsed light sintering of silane surface modified Cu oxide nanoparticle paste on Si wafer substrate for solar cell electrode *Thin Solid Films* **722** 138577
[142] Dharmadasa R, Jha M, Amos D A and Druffel T 2013 Room temperature synthesis of a copper ink for the intense pulsed light sintering of conductive copper films *ACS Appl. Mater. Interfaces* **5** 13227–34